The TOR signaling pathway regulates vegetative development, aflatoxin biosynthesis, and pathogenicity in *Aspergillus flavus*

Guoqi Li, Xiaohong Cao, Elisabeth Tumukunde, Qianhua Zeng, Shihua Wang*

State Key Laboratory of Ecological Pest Control for Fujian and Taiwan Crops, Key Laboratory of Pathogenic, Fungi and Mycotoxins of Fujian Province, School of Life Sciences, Fujian Agriculture and Forestry University, Fuzhou 350002, China

Corresponding author:
Name: Shihua Wang Professor
School of Life Sciences,
Fujian Agriculture and Forestry University
Fuzhou, Fujian, 350002, China
Phone/Fax: +86-591-83789312
E-mail: wshyyl@sina.com

Abstract

The target of rapamycin (TOR) signaling pathway is highly conserved and plays a crucial role in diverse biological processes in eukaryotes. Despite its significance, the underlying mechanism of the TOR pathway in *A. flavus* remains elusive. In this study, we comprehensively analyzed the TOR signaling pathway in *A. flavus* by identifying and characterizing nine genes that encode distinct components of this pathway. The FK506-binding protein Fkbp3 and its lysine succinylation are important for aflatoxin production and rapamycin resistance. The TorA kinase plays a pivotal role in the regulation of growth, spore production, aflatoxin biosynthesis, and responses to rapamycin and cell membrane stress. As a significant downstream effector molecule of the TorA kinase, the Sch9 kinase regulates aflatoxin B_1 (AFB_1) synthesis, osmotic and calcium stress response in *A. flavus,* and this regulation is mediated through its S_TKc, S_TK_X domains, and the ATP binding site at K340. We also showed that the Sch9 kinase may have a regulatory impact on the high-osmolarity glycerol (HOG) signaling pathway. TapA and TipA, the other downstream components of the TorA kinase, play a significant role in regulating cell wall stress response in *A. flavus*. Moreover, the members of the TapA-phosphatase complexes, SitA and Ppg1, are important for various biological processes in *A. flavus*, including vegetative growth, sclerotia formation, AFB_1 biosynthesis, and pathogenicity. We also demonstrated that SitA and Ppg1 are involved in regulating lipid droplets (LDs) biogenesis and cell wall integrity (CWI) signaling pathways. In

addition, another phosphatase complex, Nem1/Spo7, plays critical roles in hyphal development, conidiation, aflatoxin production, and lipid droplets biogenesis. Collectively, our study has provided important insight into the regulatory network of the TOR signaling pathway and has elucidated the underlying molecular mechanisms of aflatoxin biosynthesis in *A. flavus*.

Keywords: *Aspergillus flavus*; the TOR signaling pathway; aflatoxin; vegetative development

Introduction

Aspergillus flavus is a highly significant phytopathogenic fungus that frequently contaminates a diverse array of agricultural crops, leading to substantial economic losses in the food and agriculture industry and posing considerable health risks, particularly in developing countries [1]. Moreover, *A. flavus* is recognized as an opportunistic human pathogenic fungus that can cause aspergillosis in immune-compromised patients [2]. The fungus is notorious for its production of aflatoxins (AFs), which are potent secondary metabolites with toxic and carcinogenic properties and are classified among the most powerful carcinogens known in nature, with established links to liver cancer in both humans and animals [3]. Aflatoxin biosynthesis is a multifaceted and intricate biochemical process encompassing a cascade of enzymatic reactions. Although the majority of the enzyme reactions and genes involved in aflatoxin biosynthesis have been elucidated [4], the related signaling pathway network and specific regulatory mechanisms governing aflatoxin

biosynthesis remain elusive. Therefore, exploring the regulatory mechanism of the aflatoxin biosynthesis signaling pathway would provide new insights for preventing *A. flavus* and aflatoxin contamination.

In eukaryotes, the target of rapamycin (TOR) signaling pathway is highly conserved and plays essential roles in various significant biological processes, including ribosome biosynthesis, cell growth, and autophagy [5]. The serine/threonine-protein kinase Tor serves as a crucial protein component in the TOR signaling pathway, which interacts with other proteins to form multi-protein complexes [6]. In *Saccharomyces cerevisiae*, TOR exists in two distinct multiprotein functional complexes, namely TORC1 and TORC2 [7]. TORC1-mediated signaling governs cellular growth by modulating various growth-related mechanisms and exhibits sensitivity to rapamycin. Conversely, TORC2-mediated signaling primarily regulates cytoskeletal remodeling but remains unaffected by rapamycin [7]. In yeast, there are two *tor* genes, *tor1* and *tor2*, whereas in higher eukaryotes such as plants, animals, and filamentous fungi, there is only one *tor* gene [8-10].

In the fungal kingdom, the TOR signaling pathway has been extensively investigated in three prominent species: the budding yeast *S. cerevisiae* [11-12], the fission yeast *Schizosaccharomyces pombe* [13-15], and the human pathogen *Candida albicans* [16-17]. In *S. cerevisiae*, the macrolide antibiotic rapamycin forms a complex with the cytosolic protein Fkbp12, which effectively inhibits the catalytic function of the Tor kinase by interacting with its FRB domain [18]. The Tap42 phosphatase complex serves as the primary target of the Tor kinase and plays a crucial role in the

87 regulation of downstream effectors. Additionally, the Tap42 protein interacts with the
88 Tip41 protein to collaboratively modulate the activities of phosphatases, including
89 PP2A and Sit4 [19-20]. Among these, the Sit4 phosphatase is known to
90 dephosphorylate the transcription factor Gln3, thereby regulating the nitrogen source
91 metabolism pathway [21]. In addition, the AGC kinase Sch9, an immediate effector of
92 TORC1, is involved in regulating various cellular functions processes, such as
93 ribosome biosynthesis, translation initiation, and entry into the G_0 phase [22]. The TOR
94 signaling pathway has been documented in various filamentous fungi, including
95 *Fusarium graminearum* [23-24], *Magnaporthe oryzae* [25], *Phanerochaete*
96 *chrysosporium* [26], *Podospora anserine* [27], *A. nidulans* [28], *A. fumigatus* [29-30], *F.*
97 *fujikuroi* [31], *Botrytis cinerea* [32], *F. oxysporum* [33], and *Mucor circinelloides* [34].
98 However, the TOR signaling pathway in *A. flavus* remains unexplored.

99 In eukaryotic cells, the TOR signaling pathway and the mitogen-activated protein
100 kinase (MAPK) signaling pathways play an important role in regulating adaptive
101 responses to extra- and intracellular conditions [35]. Several studies have demonstrated
102 that the TOR signaling pathway interacts with various other signaling pathways, such
103 as MAPK and cell wall integrity (CWI) pathway. These pathways are recognized to
104 participate in crosstalk, forming a complex metabolic network that regulates cellular
105 processes [36-40]. However, the underlying mechanisms of multiple crosstalks between
106 the TOR and other signaling pathways in *A. flavus* remain largely unknown. Therefore,
107 we intended to identify the genes associated with the TOR signaling pathway and
108 elucidate their roles and contributions in regulating vegetative development and

109 aflatoxin biosynthesis in *A. flavus*. Our results demonstrated that the TOR signaling
110 pathway is involved in multiple cellular processes in *A. flavus*. Notably, our findings
111 revealed a complex interplay between the TOR pathway and other signaling pathways
112 (such as HOG and CWI) in *A. flavus*, which play a crucial role in regulating cellular
113 growth and survival under environmental stress conditions.

114 Results

115 Rapamycin exhibits inhibitory effects on the growth, sporulation, sclerotia 116 formation, and aflatoxin production in *A. flavus*

117 Rapamycin, a secondary metabolite synthesized by *Streptomyces hygroscopicus*,
118 exhibits efficacy in suppressing specific filamentous fungi. In *F. graminearum*,
119 rapamycin has a significant inhibitory impact on growth and asexual reproduction [23].
120 To investigate the effects of rapamycin on vegetative development, sclerotia
121 formation, and secondary metabolism in *A. flavus*, we conducted an assay to
122 determine the sensitivity of the wild-type (WT) strain to rapamycin. We observed that
123 the WT strain exhibited a high sensitivity to rapamycin. We found that 100 ng/mL of
124 rapamycin significantly inhibited mycelial growth and conidia formation (Fig. 1A, 1D,
125 1E). More importantly, the WT strain exhibited a significant reduction in sclerotia
126 formation and aflatoxin synthesis (Fig. 1B, 1C, 1F, 1G). Additionally, rapamycin
127 resulted in a significant decrease in spore germination rate and sparser conidiophores
128 (Fig. S1A, S1B). These results illustrated that the TOR signaling pathway may be
129 involved in regulating the growth, development, and secondary metabolism of *A.*

130 *flavus.* Calcofluor white is a chemifluorescent blue dye commonly employed for its
131 nonspecific binding affinity to fungal chitin. Fluorescence microscopy analysis
132 revealed a notable reduction in the blue fluorescence on the cell wall following
133 treatment with rapamycin (Fig. S1C). The intracellular lipid droplets within the
134 hyphae were labeled with BODIPY. We observed that the hyphae treated with
135 rapamycin contained more lipid droplets compared to the control group (Fig. S1D).
136 These findings suggest that the TOR pathway may play important roles in maintaining
137 cell wall integrity and facilitating the biogenesis of lipid droplets.

138 To investigate the potential regulatory role of the TOR pathway in modulating
139 the sporulation, sclerotia formation, and aflatoxin biosynthesis in *A. flavus*, we
140 examined the expression levels of conidia-related, sclerotia formation-related, and
141 aflatoxin-related genes after 3, 6, and 9 hours of treatment with rapamycin. To
142 determine the effects of rapamycin on conidiation, qRT-PCR was conducted to assess
143 the transcript levels of two conidia-related genes, *abaA* and *brlA*. We also conducted
144 qRT-PCR to evaluate the expression levels of three regulators (*nsdC*, *nsdD*, and *sclR*)
145 involved in sclerotia development, and genes involved in AFB_1 biosynthesis, such as
146 the regulatory gene *aflS*, as well as several structural genes (*aflC* and *aflQ*). The
147 strains treated with rapamycin exhibited a significant reduction in the expression
148 levels of genes related to sporulation, sclerotia formation, and aflatoxin synthesis (Fig.
149 1H, 1I, 1J). Overall, these results indicated that the TOR pathway plays a crucial role
150 in regulating the growth, sporulation, sclerotia formation, and aflatoxin biosynthesis
151 in *A. flavu*s by modulating the expression of these genes.

152 **The impact of Fkbp3 and its lysine succinylation on AFB_1 biosynthesis and**
153 **rapamycin resistance in *A. flavus***

154 FK506-binding proteins (Fkbps) belong to a highly conserved immunophilin
155 family, which are involved in various cellular functions, such as protein folding,
156 immunosuppression, signaling transduction, and transcription [41]. Fkbps function as
157 molecular switches by binding to target proteins and inducing conformational changes
158 [41]. In *S. cerevisiae*, Fkbp12 and rapamycin interact to form a complex that exerts a
159 negative regulatory effect on the activity of the Tor kinase [42]. The *fkbp12* gene
160 homologue *fprA* in *A. nidulans* shares high levels of homology with that from *S.*
161 *cerevisiae* [28]. According to the protein sequence of FprA from *A. nidulans*, four genes
162 encoding putative proteins with FK506 binding domain, named *fkbp1*
163 (AFLA_126880), *fkbp2* (AFLA_087480), *fkbp3* (AFLA_010910), and *fkbp4*
164 (AFLA_128200), have been identified from the *A. flavus* genome. We generated four
165 *fkbp* knockout strains using homologous recombination, and all *fkbp* disruption strains
166 were confirmed by PCR and sequencing analysis (Fig. S2). Phenotypic analyses
167 showed that the mycelial growth and conidia formation of all the *fkbp* mutants were
168 similar to the WT strain on the PDA medium (Fig. 2A), suggesting that Fkbps have
169 minimal influence on the process of vegetative development. We evaluated AFB_1
170 synthesis utilizing thin layer chromatography (TLC), and the findings demonstrated a
171 noteworthy reduction in AFB_1 synthesis upon deletion of Fkbp3, in comparison to the
172 WT strain (Fig. 2B, 2D). Additionally, the quantity of sclerotia exhibited a significant
173 decrease in all *fkbp* mutants compared to the WT strain (Fig. S3A, S3B). The

174 aforementioned data indicated that Fkbp3 plays a crucial role in sclerotia formation
175 and aflatoxin biosynthesis in *A. flavus*.

176 To determine the specific Fkbp responsible for rapamycin sensitivity, all mutant
177 strains were cultured on PDA solid plates amended with 100 ng/mL rapamycin. The
178 strain with disrupted *fkbp3* showed significant resistance to rapamycin, while the
179 deletion mutants of *fkbp1*, *fkbp2*, and *fkbp4* did not exhibit any alteration in resistance
180 to rapamycin (Fig. 2A, 2C). These results demonstrated that Fkbp3 serves as the
181 principal target for rapamycin in *A. flavu*s. In the FK506-sensitivity analysis, we
182 observed a significant suppression of mycelial growth and conidia formation in WT
183 strain with the addition of 10 ng/mL FK506 to the PDA medium. Additionally, the
184 deletion of *fkbp3* led to the heightened resistance to FK506 compared to the WT strain
185 (Fig. 2A, 2C). These findings suggested that Fkbp3 is mainly involved in the
186 modulation of FK506 resistance in *A. flavus*.

187 Previous studies have shown that lysine succinylation plays a significant role in
188 aflatoxin production and pathogenicity in *A. flavus* [43]. Based on the analysis of our
189 succinylome data, we have identified six reliable succinylation sites (K5, K19, K40,
190 K42, K55, and K65) on the Fkbp3 protein. To identify the function of Fkbp3
191 succinylation sites, site-directed mutations were constructed according to the
192 homologous recombination strategy. Compared to the WT strain, all point mutants
193 exhibited a similar phenotype in vegetative growth and conidiation. Interestingly, we
194 observed that the K19A mutation resulted in increased resistance to rapamycin (Fig.
195 2E, 2F). Additionally, the K19A strain exhibited a significant reduction in the

196 production of AFB_1 compared to the WT strain (Fig. 2G, 2H). These findings
197 suggested that the succinylation of Fkbp3 at K19 plays a crucial role in rapamycin
198 resistance and aflatoxin biosynthesis. Furthermore, we found that various point
199 mutants, including K40A, K42A, and K55A, exhibited reduced levels of AFB_1
200 production in comparison to the WT strain (Fig. 2G, 2H), suggesting that the
201 succinylation of Fkbp3 at other sites also contributes to AFB_1 biosynthesis in *A. flavus*.
202 The above results indicated that the K19 site likely plays a more prominent role in
203 Fkbp3 succinylation compared to other sites.

204 **The TorA kinase plays a critical role in *A. flavus***

205 In *S. cerevisiae*, the Tor kinase is known to interact with a diverse range of
206 proteins, resulting in the formation of complex structures known as TORC1 and
207 TORC2 [44]. TORC1 can detect various signals, including nutrients, growth factors,
208 and environmental stress. It plays a crucial role in regulating cellular processes such
209 as gene transcription, protein translation, ribosome synthesis, and autophagy [45]. To
210 identify the ortholog of the Tor protein in *A. flavus*, the *S. cerevisiae* Tor protein was
211 utilized as search reference in the *A. flavus* genome database using the Basic Local
212 Alignment Search Tool (https://blast.ncbi.nlm.nih.gov/Blast.cgi). The genome of *A.*
213 *flavus* contains a solitary ortholog of the *tor* gene (AFLA_044350), which encodes a
214 protein exhibiting 48.91% similarity to *S. cerevisiae* Tor2. To elucidate the role of
215 *torA* in *A. flavus*, we attempted to obtain *torA* deletion strains by homologous
216 recombination, but not successful. As an alternative approach, a mutant strain with a
217 xylose promoter mutation, referred as $^{xylP}torA$, was constructed to validate the

218 function of *torA*. Subsequent confirmation via PCR analysis ensured the integrity of
219 the mutant strain. Xylan and xylose are highly effective inducers, whereas glucose
220 strongly represses the activity of the promoter. To ascertain the impact of *torA* on *A.*
221 *flavus*, we conducted a comparative analysis of *torA* transcript levels between the
222 ^{xylP}*torA* strain and the WT strain. Our findings revealed that the *torA* transcript levels
223 in the ^{xylP}*torA* strain were markedly reduced compared to the WT strain (Figure S4A).
224 Both the WT strain and ^{xylP}*torA* mutant were cultured in YXT medium supplemented
225 with xylose and YGT medium devoid of xylose for a duration of 5 days at 37°C under
226 dark conditions. Remarkably, the ^{xylP}*torA* strain exhibited complete inability to thrive
227 in the absence of xylose, with only partial restoration of growth observed upon xylose
228 supplementation (Fig. 3A, 3D). Notably, the ^{xylP}*torA* strain also demonstrated a
229 markedly reduced growth rate on YXT compared to the WT strain (Fig. 3A, 3C).
230 Thin-layer chromatography (TLC) assays indicated a noteworthy decrease in AFB_1
231 synthesis in the ^{xylP}*torA* strain compared to the WT strain (Figure 3B, 3F).
232 Additionally, the ^{xylP}*torA* strain produced fewer conidia and sclerotium formation was
233 absent on YXT medium (Fig. 3E, S5). Interestingly, the ^{xylP}*torA* strain exhibited a
234 notable increase in sensitivity to rapamycin and SDS stress (Figure 3G, 3H).
235 Collectively, these findings suggested that the TorA kinase plays a crucial role in
236 various biological processes in *A. flavus*, including vegetative growth, asexual
237 development, sclerotia formation, response to environmental stress, and biosynthesis
238 of aflatoxins.

239 **The Sch9 kinase is involved in aflatoxin biosynthesis and the HOG pathway**

240 Sch9, a Ser/Thr kinase belonging to the AGC family, is directly phosphorylated by
241 TORC1. The phosphorylation of Sch9 is inhibited by rapamycin, as well as by carbon
242 or nitrogen starvation [22]. The putative *sch9* gene (AFLA_127440) in *A. flavus*
243 encodes a protein consisting of 706 amino acids, exhibiting 80.31% identity to the
244 Sch9 protein in *A. nidulans*. To investigate the role of Sch9 in *A. flavus*, we attempted
245 to create a *sch9* deletion mutant using a homologous recombination strategy. The
246 Δ*sch9* strain exhibited typical vegetative growth and conidiation similar to the WT
247 strain (Fig. 4B). TLC assay and quantitative analysis showed a significantly decreased
248 aflatoxin production in the Δ*sch9* strain compared to the WT strain (Fig. 4C, 4G).
249 These results indicated that Sch9 regulates aflatoxin biosynthesis in *A. flavus*.
250 In yeast, Sch9 plays an important role in the transcriptional activation of
251 osmostress inducible genes [46]. To characterize the roles of Sch9 in stress response,
252 we examined the sensitivity of the *sch9* deletion strain to various stresses including
253 osmotic stress and calcium stress. Compared with the WT strain, the Δ*sch9* mutant
254 significantly increased sensitivity to calcium stress (Fig. S6A, S6B), and decreased
255 sensitivity to osmotic stress induced by NaCl and KCl (Fig. 4D, 4H). In *A. flavus*, the
256 Sch9 kinase consists of several domains, including the protein kinase C conserved
257 region 2 (C2), protein kinase (S_TKc), AGC-kinase C-terminal (S_TK_X) domain,
258 and an ATP binding site (Fig. 4A). To explore the role of these domains and the ATP
259 binding site in Sch9 kinase, we constructed deletion strains for both domains and a
260 $sch9^{K340A}$ mutant. The results revealed that the $sch9^{\Delta S_TKc}$ strain, $sch9^{\Delta S_TK_X}$ strain, and
261 $sch9^{K340A}$ mutant exhibited similar phenotypes in osmotic stress and AFB_1 production

262 as the Δ*sch9* mutant (Fig. 4B, 4C, 4D). Therefore, we speculate that the protein kinase
263 domain, kinase C-terminal domain, and the ATP binding site at K340 play a crucial
264 role in modulating the impact of Sch9 on aflatoxin biosynthesis and stress response in
265 *A. flavus*.

266 To investigate the potential function of Sch9 in the HOG and TOR pathways in *A.*
267 *flavus*, we conducted a sensitivity analysis of the Δ*sch9* strain to rapamycin.
268 Compared to the WT strain, the *sch9* deletion strain exhibited a slightly higher
269 sensitivity to rapamycin (Fig. 4B, 4F). The MAKP Hog1 is an element of the high
270 osmolarity glycerol (HOG) pathway. To verify the connection between Sch9 and the
271 HOG-MAPK pathway, the phosphorylation levels of Hog1 kinase were measured
272 under osmotic stress (1M NaCl). Western blot analysis showed that the
273 phosphorylation level of Hog1 increased significantly in the Δ*sch9* strain (Fig. 4E).
274 This finding suggested that Sch9 plays a pivotal role in modulating the response of
275 Hog1 to osmotic stress. Taken together, these results reflected that Sch9 regulates
276 osmotic stress response via the HOG pathway in *A. flavus*.

277 **TapA and TipA participate in the regulation of cell wall stress response**

278 Tap42, a protein that associates with phosphatase 2A, serves as the direct target of
279 the Tor kinase in yeast. Tap42 plays a crucial role in various Tor functions,
280 particularly in the regulation of transcriptional processes [47]. The genome of *A. flavus*
281 contains a homolog of *tap42* named *tapA* (AFLA_092770), which is predicted to
282 encode a 355 amino-acid protein (sharing 31.9% identity with *S. cerevisiae* Tap42).
283 To further determine the function of the TapA regulator in the TOR signaling pathway

284 of *A. flavus*, we used homologous recombination to replace the original promoter with
285 the *gpdA* promoter, a well-characterized strong promoter, to construct an
286 overexpression mutant (*OE*::*tapA*). The transformants of the mutant were verified
287 using PCR. Quantitative expression analysis of the *tapA* gene in the overexpressed
288 strains revealed a substantial upregulation compared to the WT strain (Fig. S4B). Our
289 results showed that the colony diameter of the *OE*::*tapA* mutant was not significantly
290 changed compared to the WT strain (Fig. 5A). However, the rapamycin sensitivity
291 assay indicated that the *OE*::*tapA* strain displayed increased sensitivity to rapamycin
292 (Fig. 5A, 5D). We found no significant difference in aflatoxin production between the
293 *OE*::*tapA* and the WT strains (Fig. 5C, 5E), suggesting that TapA may not play a
294 direct role in the regulation of aflatoxin biosynthesis. In addition, the *OE*::*tapA* strain
295 was more sensitive to cell wall and cell membrane stress, including SDS, CFW, and
296 CR (Fig. 5B, 5F). These findings have demonstrated the significantly positive impact
297 of TapA on cell wall stress in *A. flavus*.

298 In *S. cerevisiae*, Tip41 was identified as a Tap42-interacting protein and has been
299 measured to function as a negative regulator of Tap42, which downregulates TORC1
300 signaling via activation of PP2A phosphatase [48]. The putative orthologue of *tip41* in
301 *A. flavus* is named *tipA* (AFLA_047310). The amino acid sequence of TipA exhibits a
302 similarity of 40.49% to Tip41 in *S. cerevisiae*. To elucidate the function of the TOR
303 signaling pathway protein TipA in *A. flavus*, we generated the *tipA* deletion mutants.
304 The Δ*tipA* strain exhibited a slightly reduced number of conidia produced on PDA
305 compared to the WT strain (Fig. 6A, 6C). Meanwhile, the Δ*tipA* strain exhibited

306 decreased sensitivity to rapamycin (Fig. 6A, 6E). The Δ*tipA* strain was unable to
307 produce any sclerotia (Fig. 6B, 6F). Whereas Δ*tipA* strain do not affect aflatoxin
308 production(Fig. 6D, 6G). In addition, the Δ*tipA* strain was more sensitive to the cell
309 wall and cell membrane stress, including CR and SDS (Fig. 6H, 6I). Additionally, the
310 expression levels of *nsdC* and *nsdD* exhibited a decrease in Δ*tipA* strain compared to
311 the WT strain (Fig. 6J). These results indicated that TipA is crucial for the sclerotial
312 formation and cell wall stress in *A. flavus*.

313 **Phosphatase SitA and Ppg1 are involved in growth, conidiation, and sclerotial**
314 **formation**

315 In *S. cerevisiae*, Tap42 has been identified to interact with the catalytic subunit of
316 type 2A protein phosphatases, including Pph3, Pph21, and Pph22, as well as the type
317 2A-like phosphatases Sit4 and Ppg1[19]. Phosphatase *sitA* (AFLA_108450) and *ppg1*
318 (AFLA_132610) were identified in *A. flavu*s, encoding putative orthologs of *sit4* and
319 *ppg1* in *S. cerevisiae.* To determine the biological functions of phosphatase SitA and
320 Ppg1 in *A. flavu*s, we disrupted the *sitA* and *ppg1* by homologous recombination
321 strategy. To further investigate the relationship between phosphatase SitA and Ppg1,
322 we additionally generated complemented and double deletion mutants. The vegetative
323 development phenotype analysis showed that the Δ*sitA*, Δ*ppg1*, and Δ*sitA*/Δ*ppg1*
324 strains grew significantly more slowly than the WT strain on PDA (Fig. 7A, 7D).
325 Additionally, the Δ*sitA*, Δ*ppg1*, and Δ*sitA*/Δ*ppg1* strains were more sensitive to
326 rapamycin (Fig. 7A, 7E). In addition, the Δ*sitA*, Δ*ppg1*, and Δ*sitA*/Δ*ppg1* strains
327 formed lower number of conidiophores (Fig. 7A). To gain further insight into the role

328 of SitA and Ppg1 in the process of conidiation, qRT-PCR was employed to determine
329 the transcript levels of conidiation-related genes (*abaA* and *brlA*). The expression
330 levels of the *abaA and brlA* genes were significantly downregulated in the Δ*sitA*,
331 Δ*ppg1*, and Δ*sitA*/Δ*ppg1* mutants when compared to the WT and complemented
332 strains (Fig. 7G). The analysis of sclerotial formation revealed that the Δ*sitA*, Δ*ppg1*,
333 and Δ*sitA*/Δ*ppg1* mutants exhibited a complete inability to produce any sclerotia (Fig.
334 7B, 7E). To further prove these findings, we conducted qRT-PCR to determine the
335 expression levels of three regulators (*nsdC*, *nsdD*, and *sclR*) of sclerotia development.
336 Our findings indicated that the expression levels of *nsdC*, *nsdD*, and *sclR* were all
337 significantly reduced in the Δ*sitA*, Δ*ppg1*, and Δ*sitA*/Δ*ppg1* mutants (Fig. 7H), which
338 is consistent with the observed decrease in sclerotia production in the Δ*sitA*, Δ*ppg1*,
339 and Δ*sitA*/Δ*ppg1* mutants. These results showed that SitA and Ppg1 are crucial for
340 hyphal development, conidiation, and sclerotia formation in *A. flavus*.

341 **SitA and Ppg1 play crucial roles in aflatoxin biosynthesis and pathogenicity**

342 We assayed AFB_1 biosynthesis in the Δ*sitA*, Δ*ppg1*, and Δ*sitA*/Δ*ppg1* mutants.
343 TLC analyses revealed that the Δ*sitA* and Δ*sitA*/Δ*ppg1* strains exhibited a decrease in
344 AFB_1 production, whereas the Δ*ppg1* strain showed a significant increase in AFB_1
345 production compared to the WT and complemented strains (Fig. 7C, 7F). The
346 expression levels of genes related to aflatoxin synthesis, including structural genes
347 (*aflO* and *aflP*) and regulatory genes (*aflR* and *aflS*), were determined by qRT-PCR in
348 the Δ*sitA*, Δ*ppg1*, and Δ*sitA*/Δ*ppg1* mutants. The results revealed a significant
349 downregulation of these genes in the Δ*sitA* and Δ*sitA*/Δ*ppg1* mutants, while

350 upregulated in the Δ*ppg1* mutants, compared to the WT and complemented strains
351 (Fig. 7I). These results indicated that SitA and Ppg1 play different roles in regulating
352 aflatoxin biosynthesis in *A. flavus*.

353 We conducted pathogenicity tests on peanuts and maize to examine the
354 pathogenicity of the phosphatases SitA and Ppg1 on crops. The results showed that
355 the WT and complemented strains demonstrated complete virulence on all peanut and
356 maize seeds. In contrast, the Δ*sitA*, Δ*ppg1*, and Δ*sitA*/Δ*ppg1* mutants displayed
357 compromised colonization on peanut and maize seeds (Fig. 8A). In addition, the
358 number of conidial productions in these mutants on the infected peanut seeds also
359 dramatically decreased compared to those of the WT and complemented strains (Fig.
360 8C). The thin-layer chromatography analyses revealed that the Δ*ppg1* mutant
361 exhibited increased production of AFB_1 in peanuts and maize. Conversely, the levels
362 of aflatoxin produced by the Δ*sitA* and Δ*sitA*/Δ*ppg1* mutants on peanut and maize
363 were significantly reduced compared to the WT and complemented strains (Fig. 8B,
364 8D). This observation aligns with the above results of aflatoxin biosynthesis from all
365 mutant strains in the YES medium. All these data showed that SitA and Ppg1 are
366 crucial for crop seeds' pathogenicity.

367 **SitA and Ppg1 are involved in regulating cell wall integrity**

368 To explore the role of phosphatases SitA and Ppg1 in response to cell wall stress,
369 all strains were cultivated on PDA amended with CFW, CR, and SDS. We found that
370 the relative growth inhibition of Δ*sitA*, Δ*ppg1*, and Δ*sitA*/Δ*ppg1* mutants induced by
371 cell wall stress was significantly increased compared to the WT and complemented

372 strains (Fig. 9A, 9B). Further investigations using qRT-PCR revealed a notable
373 reduction in the expression levels of genes related to the synthesis of cell walls,
374 specifically chitin synthase genes *chsA*, *chsD*, and *chsE* in the Δ*sitA*, Δ*ppg1*, and
375 Δ*sitA*/Δ*ppg1* strains (Fig. 9C). Western blot analysis also revealed that the
376 phosphorylation level of Slt2 was significantly elevated in the Δ*sitA*, Δ*ppg1*, and
377 Δ*sitA*/Δ*ppg1* strains under cell wall stress (200 μg/ml CFW) (Fig. 9D). In conclusion,
378 the phosphatases SitA and Ppg1 play a crucial role in regulating cell wall integrity.

379 **The phosphatase complex Nem1/Spo7 is important for growth, aflatoxin**
380 **biosynthesis, and LD biogenesis**

381 Lipid droplets (LDs) are highly dynamic spherical organelles, which appear in
382 the cytosol of most eukaryotic cell types[49]. Rapamycin treatment led to the
383 accumulation of lipid droplets in various filamentous fungi [24]. The FgTOR pathway
384 regulates the phosphorylation status of FgNem1 mainly via the
385 FgPpg1/Sit4-FgCak1/other kinase cascade in *F. graminearum* [24]. In this study, we
386 observed that the treatment of hyphae with rapamycin resulted in the accumulation of
387 LD biogenesis (Fig. 10A). This finding suggested that the TOR pathway may regulate
388 the LD biogenesis. However, the underlying regulatory mechanism of LD
389 biosynthesis remain largely unknown in *A. flavu*s. To investigate the regulatory
390 mechanism of the TOR pathway in *A. flavus* that controls LD biogenesis, we
391 examined LD accumulation in Δ*sch9*, Δ*sitA*, and Δ*ppg1* mutants. BODIPY staining
392 assays revealed that LD biogenesis was not observed in the Δ*sitA* and Δ*ppg1* strains
393 upon treatment with rapamycin, in contrast to the WT and Δ*sch9* strains (Fig. 10A,

394 10B, 10C, 10D). These results indicated that LD biogenesis induced by rapamycin is
395 predominantly reliant on the phosphatases SitA and Ppg1 in *A. flavus*. In *F.*
396 *graminearum*, the phosphatase FgNem1/FgSpo7 complex was involved in the
397 induction of LD biogenesis by rapamycin[24]. Phosphatase *nem1* (AFLA_002649) and
398 *spo7* (AFLA_028590) were identified in *A. flavu*s, which encode putative orthologs of
399 *nem1* and *spo7* in *F. graminearum.* To examine the role of the *nem1* and *spo7* genes in
400 *A. flavus*, we generated Δ*nem1* and Δ*spo7* mutants using homologous recombination.
401 The Δ*nem1* and Δ*spo7* mutants displayed a notable reduction in both vegetative
402 growth and conidiation compared to the WT strain (Fig. 11A, 11C, 11D). TLC assay
403 revealed a significantly decreased aflatoxin production in the Δ*nem1* and Δ*spo7*
404 compared to the WT strain (Fig. 11B). In addition, BODIPY staining showed no
405 visible lipid droplets in the hyphae of Δ*nem1* and Δ*spo7* after rapamycin treatment
406 (Fig. 9E). Taken together, these results indicated that Nem1/Spo7 are involved in
407 vegetative growth, conidiation, aflatoxin production, and LD biogenesis.

408 **Discussion**

409 Aflatoxins (AFs) are a class of toxic secondary metabolites synthesized by *A.*
410 *flavus*, including aflatoxin B_1, B_2, G_1, and G_2, among which AFB_1 has been regarded
411 as the most pathogenic and toxic aflatoxin[50]. Therefore, understanding the regulatory
412 mechanisms involved in fungal secondary metabolites biosynthesis would be
413 instrumental for effectively addressing aflatoxin control in *A. flavus*. In this study, we
414 demonstrated that the target of rapamycin (TOR) signaling pathway plays a pivotal

415 role in regulating growth, sporulation, sclerotia formation, aflatoxin production, and
416 various stress responses in *A. flavus*. Through conducting functional studies on genes
417 within the TOR signaling pathway, we explored the conservation and complexity
418 exhibited by the TOR signaling pathway in *A. flavu*s. In addition, we constructed a
419 crosstalk network between the TOR and other signaling pathways (HOG, CWI) and
420 analyzed the specific regulatory process. We proposed that the TOR signaling
421 pathway interacts with multiple signaling pathways, including HOG and CWI
422 pathways, to modulate the cellular responses to diverse environmental stresses (Fig.
423 10).

424 Our findings indicated that the TOR signaling pathway is pivotal in *A. flavus*,
425 we have observed that rapamycin has a significant impact on the growth and
426 sporulation of *A. flavus* (Fig. 1A). Additionally, it exhibits a strong inhibitory effect on
427 sclerotia production and aflatoxin biosynthesis (Fig. 1B, 1C). The inhibitory effect has
428 been documented in various fungal species, including *Candida albicans* [51],
429 *Cryptococcus neoformans* [51], *Podospora anserine* [27], *A. nidulans* [28], *Magnaporthe*
430 *oryzae* [39], and *F. graminearum* [23]. This suggested that the TOR signaling pathway
431 may have a conserved function in filamentous fungi. The number of FK506-binding
432 proteins varies among different species: there are four Fkbps proteins in *S. cerevisiae*
433 and three Fkbps proteins in *S. pombe* [52]. In *S. cerevisiae*, rapamycin can bind to Fkbp
434 protein, resulting in the irreversible inhibition of the G_1 phase of the cell cycle and the
435 regulation of cell growth [53]. In *A. nidulans,* the *fkbp12* gene homologue *fprA* displays
436 considerable sequence similarity with homologues identified in the *S. cerevisiae* [28].

437 In this study, based on the homologous alignment of the protein sequence of FprA, it
438 was observed that four *fkbp* genes are present in *A. flavus*. Among these, deletion of
439 *fkbp3* exhibited enhanced tolerance to rapamycin (Fig. 2A). So we speculated that
440 rapamycin forms a complex with Fkbp3 in *A. flavus*, subsequently targeting
441 downstream target genes to exert its biological function. We found that Fkbp3 is
442 involved in sclerotia formation and aflatoxin biosynthesis in *A. flavus* (Fig. 2A, S3),
443 and subsequent analysis revealed that the underlying mechanism may be associated
444 with succinylation modification. The succinylation sites of Fkbp3 were identified
445 through the utilization of succinylation proteomics data. By constructing point mutant
446 strains and conducting phenotype experiments, we found that the succinylation of
447 Fkbp3 at residue K19 is involved in rapamycin resistance and aflatoxin biosynthesis
448 (Fig. 2E, 2G). Our results provided new insights to the understanding of
449 post-translational modifications in the regulation of TOR pathway components.
450 Previous studies have demonstrated that Fkbp12 has been identified as the receptor
451 for FK506 and rapamycin, which inhibits calcineurin and target rapamycin complex 1
452 (TORC1), respectively [53]. The deletion of Fkbp12 confers the resistance to
453 rapamycin in *C. albicans* [51] and *C. neoformans* [51]. The entomopathogenic fungus
454 *Beauveria bassiana* contains three putative *fkbp* genes, and disruption of *Bbfkbp12*
455 significantly increases the resistance to rapamycin and FK506 [54]. The plant
456 pathogenic fungus *F. graminearum* harbors three Fkbps proteins, among which
457 deletion of *Fgfkbp12* leads to resistance to rapamycin [23]. Thus, we propose that these
458 Fkbps may exhibit analogous functionalities in conferring resistance to rapamycin. In

459 *Botrytis cinerea*, deletion of *Bcfkbp12* caused a reduction of the virulence of strain T4,
460 while knockout of the *fkbp12* gene did not affect the pathogenic development of strain
461 B05.10 [32]. These findings demonstrated that the *fkbp12* homologous genes exhibited
462 conservation in terms of rapamycin resistance. However, there is significant variation
463 in other biological functions among fungal species, which may be attributed to species
464 or strain evolutionary divergence. Our study indicated the pivotal role of Fkbp3 in
465 modulating the effects of rapamycin on *A. flavus*, Fkbp3 is also crucial for aflatoxin
466 biosynthesis. Targeted inhibition of Fkbp3 could potentially suppress aflatoxin
467 production, given its significance, Fkbp3 can be developed as a drug target to reduce
468 aflatoxin biosynthesis, thereby reducing the risk of aflatoxin contamination in
469 agricultural products.

470 The Tor kinase functions as a fundamental component of the TOR signaling
471 pathway, which exhibits evolutionary conservation across fungi, plants, and mammals
472 [55]. In *S. cerevisiae*, the Tor kinase can interact with a diverse range of proteins,
473 resulting in the formation of complex structures known as TORC1 and TORC2 [44].
474 TORC1 can detect various signals, including nutrients, growth factors, and
475 environmental stress. It plays a crucial role in regulating cellular processes such as
476 gene transcription, protein translation, ribosome synthesis, and autophagy [45]. A
477 characteristic that distinguishes TORC1 is its interaction with KOG1 (Raptor in
478 mammals) and its sensitivity to the rapamycin-FKBP12 complex [56]. The Tor kinase
479 is widely conserved both in terms of its structural characteristics and its role as the
480 target of Fkbp-rapamycin [57]. Typically, the Tor kinase exhibits similar structural

481 characteristics, including the HEAT-like, FAT, FRB, kinase, and FATC domains [57].
482 The FRB domain is the binding region of the Fkbp-rapamycin complex, and
483 rapamycin resistance is usually caused by the disruption of the FRB domain [45].
484 Homology analysis and phylogenetic studies have identified a single predicted *torA*
485 gene within the *A. flavus* genome. To elucidate the functional role of *torA* in *A. flavus*,
486 our initial approach involved an attempt to generate an *torA* deletion strain through
487 homologous recombination. However, these efforts were unsuccessful. We speculated
488 that the deletion of the *torA* gene may be lethal in *A. flavus*. This observation aligns
489 with the situation observed in *F. graminearum* [23]. Therefore, to investigate the
490 function of TorA in *A. flavus*, we constructed a mutant strain (^{xylP}*torA*) using an
491 xylose-inducible promoter, which allows for conditional induction with the addition
492 of xylose. We observed that the ^{xylP}*torA* mutant is completely unable to grow in YGT
493 medium without xylose, whereas partial growth is restored in YXT medium with the
494 addition of xylose (Fig. 3A). These results indicated that TorA is essential for the
495 growth of *A. flavus*. We also discovered that the Tor kinase is involved in the
496 vegetative growth, asexual development and aflatoxin production of *A. flavus* (Fig.
497 3A, 3B). In addition, the the ^{xylP}*torA* mutant shows a high sensitivity to rapamycin and
498 SDS (Fig. 3A). Our findings have demonstrated that the TorA kinase plays a crucial
499 role in the processes of morphogenesis, aflatoxin biosynthesis, and multiple stress
500 responses in *A. flavus*. Previous findings demonstrated that the Tor kinase could
501 function as a molecular switch connecting an iron cue to defend against pathogen
502 infection in *C. elegans* [58]. In *A. fumigatus*, the Tor kinase represents a central

503 regulatory node controlling genes and proteins involved in nutrient sensing, stress
504 response, cell cycle progression, protein biosynthesis, and degradation, as well as
505 adaptation to low iron conditions[59]. In summary, the Tor kinase acts as a central
506 regulator in the TOR signaling pathway, playing a crucial role in the regulation of the
507 cell cycle, protein synthesis, and cellular energy metabolism. Its influence on key
508 cellular processes makes it a promising target for future research to control fungal
509 growth and aflatoxin production.

510 The serine/threonine protein kinase Sch9, a critical downstream effector of
511 TORC1 in *S. cerevisiae*, has been extensively studied for its roles in stress resistance,
512 longevity, and nutrient sensing [46]. In addition, the TORC1-Sch9 pathway is also
513 recognized as crucial mediator of chronological lifespan [46]. In filamentous fungi, an
514 intricate network of interactions exists between the TOR and HOG pathways. In *F.*
515 *graminearum* [38], FgSch9 and FgHog1 mutants displayed increased susceptibility to
516 osmotic and oxidative stresses. The phosphorylation level of FgHog1 increased
517 significantly in FgSch9 mutant. Additionally, the affinity capture-MS assay showed
518 that the Tor kinase was among the proteins co-purifying with FgSch9. These results
519 suggested that FgSch9 serves as an intermediary for the TOR and HOG signaling
520 pathways [38]. Furthermore, FgSch9 plays a crucial role in the regulation of various
521 biological processes such as hyphal differentiation, asexual development, virulence,
522 and DON biosynthesis[38]. In *A. fumigatus*, the SchA mutant was sensitive to
523 rapamycin, high concentrations of calcium and hyperosmotic stress, and SchA was
524 involved in iron metabolism. The SchA mutant exhibited enhanced phosphorylation

525 of SakA in response to osmotic stress [29]. In this study, we discovered that Sch9 is
526 involved in regulating aflatoxin biosynthesis (Fig. 4C), and responses to osmotic and
527 rapamycin stress (Fig. 4B, 4D). The S_TKc domain deletion strain (*sch9*$^{\Delta S_TKc}$),
528 S_TK_X domain deletion strain (*sch9*$^{\Delta S_TK_X}$), and *sch9*^{K340A} mutant displayed a
529 similar phenotype to the Δ*sch9* strain (Fig. 4B, 4C, 4D). These findings revealed that
530 Sch9 plays a significant role in the biological synthesis of aflatoxin and in responding
531 to various stresses. This role is primarily mediated through its kinase domain,
532 kinase-C domain, and ATP binding site K340. We also found that the phosphorylation
533 level of Hog1 increased significantly in the Δ*sch9* strain under osmotic stress (Fig.
534 4E). Based on the above results, we hypothesized that Sch9 was involved in the
535 osmotic stress response by modulating the HOG pathway in *A. flavus*.

536 The phosphorylation state of Tap42 is crucial for its interaction with PP2A
537 subunits and is regulated by a balance between Tor-mediated phosphorylation and
538 Cdc55/Tpd3-mediated dephosphorylation in yeast [60]. The genome of *A. flavus*
539 contains a homolog of *tap42* named *tapA* (AFLA_092770), which is predicted to
540 encode a 355 amino-acid protein (sharing 31.9% identity with *S. cerevisiae* Tap42).
541 To further determine the function of the TapA regulator in the TOR signaling pathway
542 of *A. flavus*, we conducted targeted gene deletion experiments on *tapA*. We failed to
543 obtain a null mutant, we hypothesised that *tapA* knockout was lethal in *A. flavus*. To
544 investigate the function of TapA, we employed homologous recombination, to replace
545 the native promoter with the strong *gpdA* promoter, thereby constructing an
546 overexpression strain (*OE*::*tapA*) with the enhanced promoter. Compared with WT

547 strain, *OE*::*tapA* strain were more sensitive to rapamycin and SDS stress, indicating
548 that *tapA* gene plays an important role in regulating cell wall stress (Fig. 5B, 5F). In *S.*
549 *pombe*, the protein Tip41, which interacts with Tap42, plays a significant role in the
550 cellular responses to nitrogen sources by regulating type 2A phosphatases [61]. In *S.*
551 *cerevisiae*, Tap42-phosphatase complexes associate with TORC1, whereas Tip41
552 functions to attenuate TORC1 signaling by stimulating the PP2A phosphatase [48].
553 Unlike its yeast counterpart Tip41, TIPRL, a mammalian Tip41-like protein, exerts a
554 positive influence on mTORC1 signaling by interacting with PP2Ac [62]. While some
555 functions of Tap42 and its binding partners Tip41 may be conserved, the interaction
556 between Tip41 and Tap42 was not observed in the filamentous fungi. The yeast
557 two-hybrid (Y2H) assay showed that FgTip41 interacts with the phosphatase FgPpg1
558 rather than FgTap42, while the FgTap42 bind with phosphatases FgPp2A, implying
559 that FgTap42, FgPpg1, and FgTip41 form a heterotrimer in *F. graminearum* [23]. In the
560 rice blast fungus *M. oryzae*, MoTip41 does not interact with MoTap42. However,
561 MoTip41 can bind with the phosphatase MoPpe1, thereby facilitating crosstalk
562 between the TOR pathway and the cell wall integrity pathway [40]. In *A. flavus,* the
563 *OE*::*tapA* and Δ*tipA* strains showed increased sensitivity to cell wall stress compared
564 with the WT strain(Fig. 5B, 6H). Based on the conserved roles of Tap42 and Tip41 in
565 yeast and other filamentous fungi, we hypothesize that TapA and TipA in *A. flavus*
566 also participate in cell wall integrity pathway. In summary, our study provided
567 important insights into the role of TapA and TipA in the TOR signaling pathway of *A.*
568 *flavus*, particularly in relation to cell wall stress. However, their interaction and

569 implications for TOR and CWI signaling in *A. flavus* remain to be elucidated.

570 In *S. cerevisiae*, Tap42 can bind and regulate various PP2A phosphatases,
571 including Pph3, Pph21, Pph22, Sit4, and Ppg1. This interaction plays a crucial role in
572 the TOR signaling pathway, particularly in response to rapamycin treatment or
573 nutrient deprivation [48]. These phosphatases play important roles in other fungi and
574 are involved in a variety of cellular processes, including growth, morphogenesis, and
575 virulence. For example, the phosphatase Sit4 plays a crucial role in regulating cell
576 growth, morphogenesis, and virulence in *C. albicans* [63]. Similarly, FgSit4 and
577 FgPpg1 are associated with various cellular processes, including mycelial growth,
578 conidiation, DON biosynthesis, and virulence in *F. graminearum* [23]. These findings
579 indicated the conserved role of PP2A phosphatases in fungal biology. In addition to
580 their roles in growth and development, FgSit4 and FgPpg1 are involved in the
581 regulation of various signaling pathways, such as the CWI pathway and lipid droplets
582 biogenesis regulation pathway [23]. In this study, we found that the phosphatase SitA
583 and Ppg1 play critical role in vegetative growth, conidiation, sclerotia formation, and
584 aflatoxin biosynthesis in *A. flavus* (Fig. 7A, 7B, 7C). Additionally, the phosphatase
585 SitA and Ppg1 also affect pathogenicity and LD biogenesis (Fig. 8A, 10C, 10D). This
586 highlights the multifaceted influence of PP2A phosphatases on cellular signaling.

587 After the deletion of the *sitA* and *ppg1* genes, the expression level of genes related
588 to cell wall synthesis has decreased significantly, resulting in damage to the cell wall
589 and showing a higher sensitivity to cell wall integrity stress (Fig. 9C). Western
590 blotting results showed that the phosphorylation level of MAPK kinase Slt2 has

591 increased significantly in the Δ*sitA* and Δ*ppg1* strains under cell wall stress, indicating
592 that SitA and Ppg1 exert a negative regulatory effect on the CWI pathway (Fig. 9D).
593 In *M. oryzae*, MoPpe1 and MoSap1 serve as an adaptor complex that connects the
594 CWI and TOR signaling pathways. The activation of the TOR pathway leads to the
595 inhibition of the CWI pathway, highlighting a critical regulatory interplay between
596 these two pathways in fungal biology [39]. We speculated that SitA and Ppg1 might
597 exhibit similar regulation within the CWI and TOR pathways across different fungal
598 species. In addition, the phosphatase MoPpe1 interacts with the
599 phosphatase-associated protein MoTip41, facilitating the exchange of information
600 between the TOR and CWI signaling pathways [39]. These results suggested that the
601 phosphatase Ppe1 engages in interactions with various proteins to effectively
602 coordinate the TOR and CWI signaling pathways, thereby regulating the growth and
603 pathogenicity of the rice blast fungus *M. oryzae* [39]. Given the conserved functions of
604 PP2A phosphatases and the observed roles of SitA, Ppg1, TapA, and TipA in cell wall
605 stress response, we hypothesized that TapA-phosphatase complexes may collaborate
606 to regulate cell wall integrity processes in *A. flavus*. This hypothesis is supported by
607 the similar functions exhibited by these proteins.

608 In *F. graminearum,* the phosphatase complex FgNem1/Spo7-FgPah1 cascade
609 plays significant roles in fungal development, DON production, and lipid droplet (LD)
610 biogenesis [24]. Our study explored the conservation and functional significance of
611 Nem1 and Spo7 homologs in *A. flavus*, revealing their pivotal roles in vegetative
612 growth and secondary metabolism (Fig. 11A, 11B). Our results indicated that lipid

613 droplet biogenesis is facilitated by the Nem1/Spo7 and SitA/Ppg1 pathways in *A.*
614 *flavus* (Fig. 10C, 10D, 10E). These observations suggested a conserved and central
615 role for PP2A phosphatases as core regulators within the LD biogenesis signaling
616 network, highlighting their importance in cellular lipid metabolism and energy storage.
617 While our findings underscored the significance of phosphatases in LD biogenesis, it
618 is also plausible that other kinases contribute to the regulation of this process. To gain
619 a comprehensive understanding of the precise molecular mechanism, it is essential to
620 investigate the interplay between phosphatases and other kinases.

621 In conclusion, we identified the complex regulatory network that provides
622 important insight into the interplay between the TOR, HOG, and CWI signaling
623 pathways, and how they collectively regulate the development, aflatoxin biosynthesis,
624 and pathogenicity of *A. flavus*. By elucidating the functions of genes associated with
625 the TOR signaling pathway, our research could establish a solid foundation for
626 comprehending the molecular mechanism underlying the aflatoxin biosynthesis of *A.*
627 *flavus*. Our results could also contribute to the development of targeted strategies to
628 manage aflatoxin contamination and mitigate the impact of *A. flavus* infections.

629 Materials and methods

630 Strains and cultural conditions

631 The *A. flavus* strains in this study were shown in Table S1. All strains were
632 cultivated on four different types of agar media: potato dextrose agar (PDA), yeast
633 extract-sucrose agar (YES), yeast extract-glucose agar (YGT) and yeast extract-xylose

634 agar (YXT). The growth and conidiation assays were conducted at 37°C. Additionally,
635 aflatoxin production was assessed using YES and YXT liquid medium at 29°C.

636 **Constructions of gene deletion and complemented mutants**

637 The construction of gene deletion and complemented strains was carried out
638 using the SOE-PCR strategy, following previously established protocols [64]. To
639 generate the ^{xylP}*torA* mutant of *A. flavus* , an *torA* xylose promoter mutant cassette was
640 synthesized via overlapping extension PCR. This cassette was designed to incorporate
641 an upstream fragment of the *torA* gene, a selectable marker gene (*pyrG* from
642 *Aspergillus fumigatus*), the xyIP xylose-inducible promoter [65], and a fragment of the
643 *torA* coding sequence. Subsequently, this composite cassette was integrated into the *A.*
644 *flavus* genome via homologous recombination, specifically replacing the native *torA*
645 promoter with the inducible xylose promoter. To construct over-expression cassettes
646 for the *tapA* gene , we utilized a molecular cloning strategy that entailed the fusion of
647 PCR-amplified fragments from the *pyrG*-selectable marker and the *gpdA* promoter.
648 Subsequently, employing a homologous recombination approach, we inserted this
649 composite fragment upstream of the *tapA* gene, effectively replacing its native
650 promoter with the stronger *gpdA* promoter. The primers utilized for the amplification
651 of the flanking sequences of each gene can be found in Table S2. The putative gene
652 deletion mutants were validated through PCR assays using the appropriate primers
653 (Fig. S2), and their confirmation was subsequently obtained through sequencing
654 analysis.

655 **Growth, conidiation, and sclerotia analysis**

656 To evaluate mycelial growth and conidia formation, 1 μL of 10^6 spores/mL conidia
657 of all strains was point inoculated onto the center of the PDA medium, and then
658 cultured at 37°C for 5 days in the dark. The conidia were washed with 0.07%
659 Tween-20 and counted using a hemocytometer and microscope [43]. For sclerotia
660 formation analysis, each strain was inoculated and cultivated on CM and YXT agar
661 medium at 37°C in the dark for 7 days, and then 75% ethanol was used to wash away
662 mycelia and conidia on the surface of the medium [66]. These assays were repeated at
663 least three times.

664 **Extraction and quantitative analysis of aflatoxin**

665 To extract and quantify aflatoxins (AFs) production, 1 μL of 10^6 spores/mL
666 conidia of all strains was point inoculated onto liquid YES medium, and cultures were
667 then incubated at 29°C in the dark for 6 days. AFs were extracted from the media and
668 detected using thin layer chromatography (TLC) [66]. In addition, the standard AFB_1
669 was employed for visual comparison, and AFs were quantitatively analyzed using the
670 Image J tool. The assays were repeated at least three times.

671 **Stress assay**

672 To determine the roles of the gene in *A. flavus* responsing to various
673 environmental stresses, 1 μL of 10^6 spores/mL conidia of all strains were point
674 inoculated onto these PDA solid plates supplemented with various agents. These
675 agents included 1M NaCl, 1M KCl, and 1M $CaCl_2$ for inducing osmotic stress, as
676 well as 100 μg/mL or 300 μg/mL SDS, 200 μg/mL Calcofluor white (CFW), and 200
677 μg/mL Congo red (CR) for inducing cell wall stress. After 5 days of incubation at

678 37℃ in the dark, the relative rates of inhibition were determined [67]. The assays were
679 repeated at least three times.

680 **Seeds infection assays**

681 To measure the pathogenicity of *A. flavus*, all peanut and maize seeds were
682 washed in 0.05% sodium hypochlorite, 75% ethanol, and sterile water, respectively.
683 Subsequently, all peanut and maize seeds were immersed in sterile water containing
684 10^6 spores/mL of all strains at 29℃ in the dark for 60 min. After the conidia adhesion,
685 the seeds were cultured at 29℃ for 6 days in the dark [67].

686 **Quantitative RT-PCR**

687 For the real-time quantitative PCR (qPCR) assays, the *A. flavus* strains were
688 cultivated in the PDA medium at 29℃ for 3 days in the dark. Total RNA was
689 extracted from the mycelia of all strains, and cDNA was synthesized with the First
690 Strand cDNA Synthesis Kit, and then the cDNA was used as the template for
691 qRT-PCR analysis with SYBR Green qPCR mix. The relative transcript level of each
692 gene was calculated by the $2^{-\Delta\Delta CT}$method [68].

693 **Western blot analysis**

694 To extract the total protein, the mycelia of each strain were cultivated in YES
695 liquid medium for 48 h, then the sample was grinded under liquid nitrogen to a fine
696 powder and transferred to a 1.5 mL microcentrifuge tube added with RIPA lysis buffer
697 and 1 mM PMSF protease inhibitor. Proteins were separated by 12% SDS-PAGE and
698 transferred onto a polyvinylidene fluoride (PVDF) membrane. Phosphorylation levels
699 of Hog1 and Slt2 were detected by Phospho-p38 MAPK antibody (Cell Signaling

700 Technology, Boston, MA, USA) and Phospho-p44/42 MAPK (Erk 1/2) antibody (Cell
701 signaling Technology, MA, USA), respectively. The experiment was conducted three
702 times independently.

703 **Statistical analysis**

704 All data were measured with means ± standard deviation (SD) of three biological
705 replicates. Graph Pad Prism 7 software was used for conducting statistical and
706 significance analysis, and p-values < 0.05 represented statistical significance.
707 Student's *t*-test was used to compare the two means for differences, whereas Tukey's
708 multiple comparisons were used for testing multiple comparisons.

709 Acknowledgments

710 The authors also thank Zhenhong Zhuang, Jun Yuan, Yu Wang, Kunzhi Jia,
711 Xiuna Wang, and Xinyi Nie for their help in the experiments. This work was
712 supported by the National Natural Science Foundation of China (Grant No.
713 31972214).

714 Author contributions

715 Guoqi Li and Xiaohong Cao designed the experiments. Guoqi Li, Xiaohong Cao,
716 and Qianhua Zeng performed the experiments. Guoqi Li, Xiaohong Cao, and Shihua
717 Wang analyzed the data. Guoqi Li, Elisabeth Tumukunde, and Shihua Wang wrote the
718 manuscript. The manuscript was discussed and revised by all the authors.

719 References

720 [1] Klich MA. *Aspergillus flavus*: the major producer of aflatoxin. Mol Plant Pathol.

721 2007; 8(6): 713-22.

722 [2] Hedayati MT, Pasqualotto AC, Warn PA, et al. *Aspergillus flavus*: human
723 pathogen, allergen and mycotoxin producer. Microbiology (Reading). 2007;
724 153(Pt 6): 1677-1692.

725 [3] Khan R, Ghazali FM, Mahyudin NA, et al. Biocontrol of aflatoxins using
726 non-aflatoxigenic *Aspergillus flavus*: a literature review. J Fungi (Basel). 2021;
727 7(5): 381.

728 [4] Yabe K, Nakajima H. Enzyme reactions and genes in aflatoxin biosynthesis. Appl
729 Microbiol Biotechnol. 2004; 64(6): 745-55.

730 [5] Wullschleger S, Loewith R, Hall MN. TOR signaling in growth and metabolism.
731 Cell. 2006; 124(3): 471-84.

732 [6] De Virgilio C, Loewith R. The TOR signalling network from yeast to man. Int J
733 Biochem Cell Biol. 2006; 38(9): 1476-1481.

734 [7] Loewith R, Jacinto E, Wullschleger S, et al. Two TOR complexes, only one of
735 which is rapamycin sensitive, have distinct roles in cell growth control. Mol Cell.
736 2002; 10(3): 457-68.

737 [8] Beauchamp EM, Platanias LC. The evolution of the TOR pathway and its role in
738 cancer. Oncogene. 2013 Aug 22; 32(34): 3923-32.

739 [9] Fu L, Liu Y, Qin G, et al. The TOR-EIN2 axis mediates nuclear signalling to
740 modulate plant growth. Nature. 2021; 591(7849): 288-292.

741 [10] Teichert S, Wottawa M, Schönig B, et al. Role of the *Fusarium fujikuroi* TOR
742 kinase in nitrogen regulation and secondary metabolism. Eukaryot Cell. 2006;

743 5(10): 1807-1819.

744 [11] Crespo JL, Hall MN. Elucidating TOR signaling and rapamycin action: lessons
745 from *Saccharomyces cerevisiae*. Microbiol Mol Biol Rev. 2002; 66(4): 579-591.

746 [12] Rohde JR, Bastidas R, Puria R, et al. Nutritional control via Tor signaling in
747 *Saccharomyces cerevisiae*. Curr Opin Microbiol. 2008; 11(2): 153-60.

748 [13] Ishiguro J, Shibahara K, Ueda Y, et al. Fission yeast TOR signaling is essential
749 for the down-regulation of a hyperactivated stress-response MAP kinase under
750 salt stress. Mol Genet Genomics. 2013; 288(1-2): 63-75.

751 [14] Otsubo Y, Yamamato M. TOR signaling in fission yeast. Crit Rev Biochem Mol
752 Biol. 2008; 43(4): 277-83.

753 [15] Petersen J. TOR signalling regulates mitotic commitment through stress-activated
754 MAPK and Polo kinase in response to nutrient stress. Biochem Soc Trans. 2009;
755 37(Pt1): 273-7.

756 [16] Bastidas RJ, Heitman J, Cardenas ME. The protein kinase Tor1 regulates adhesin
757 gene expression in *Candida albicans*. PLoS Pathog. 2009; 5(2): e1000294.

758 [17] Liu NN, Flanagan PR, Zeng J, et al. Phosphate is the third nutrient monitored by
759 TOR in *Candida albicans* and provides a target for fungal-specific indirect TOR
760 inhibition. Proc Natl Acad Sci U S A. 2017; 114(24): 6346-6351.

761 [18] Hu K, Guo S, Yan G, et al. Ubiquitin regulates TORC1 in yeast *Saccharomyces*
762 *cerevisiae*. Mol Microbiol. 2016; 100(2): 303-314.

763 [19] Wang H, Wang X, Jiang Y. Interaction with Tap42 is required for the essential
764 function of Sit4 and type 2A phosphatases. Mol Biol Cell. 2003; 14(11): 4342-51.

765 [20] Yan G, Shen X, Jiang Y. Rapamycin activates Tap42-associated phosphatases by
766 abrogating their association with Tor complex 1. EMBO J. 2006; 25(15):
767 3546-55.
768 [21] Tate JJ, Tolley EA, Cooper TG. Sit4 and PP2A dephosphorylate nitrogen
769 catabolite repression-sensitive Gln3 when TorC1 is up- as well as downregulated.
770 Genetics. 2019; 212(4): 1205-1225.
771 [22] Urban J, Soulard A, Huber A, et al. Sch9 is a major target of TORC1 in
772 *Saccharomyces cerevisiae*. Mol Cell. 2007; 26(5): 663-74.
773 [23] Yu F, Gu Q, Yun Y, et al. The TOR signaling pathway regulates vegetative
774 development and virulence in *Fusarium graminearum*. New Phytol. 2014; 203(1):
775 219-32.
776 [24] Liu N, Yun Y, Yin Y, et al. Lipid droplet biogenesis regulated by the
777 FgNem1/Spo7-FgPah1 phosphatase cascade plays critical roles in fungal
778 development and virulence in *Fusarium graminearum*. New Phytol. 2019; 223(1):
779 412-429.
780 [25] Sun G, Elowsky C, Li G, et al. TOR-autophagy branch signaling via Imp1
781 dictates plant-microbe biotrophic interface longevity. PLoS Genet. 2018; 14(11):
782 e1007814.
783 [26] Nguyen DV, Roret T, Fernandez-Gonzalez A, et al. Target of rapamycin pathway
784 in the white-rot fungus *Phanerochaete chrysosporium*. PLoS One. 2020; 15(2):
785 e0224776.
786 [27] Dementhon K, Paoletti M, Pinan-Lucarré B, et al. Rapamycin mimics the

787 incompatibility reaction in the fungus *Podospora anserina*. Eukaryot Cell. 2003;
788 2(2): 238-46.
789 [28] Fitzgibbon GJ, Morozov IY, Jones MG, et al. Genetic analysis of the TOR
790 pathway in *Aspergillus nidulans*. Eukaryot Cell. 2005; 4(9): 1595-8.
791 [29] Alves de Castro P, Dos Reis TF, et al. The *Aspergillus fumigatus* SchA^{SCH9} kinase
792 modulates SakA^{HOG1} MAP kinase activity and it is essential for virulence. Mol
793 Microbiol. 2016; 102(4): 642-671.
794 [30] Baldin C, Valiante V, Krüger T, et al. Comparative proteomics of a tor inducible
795 *Aspergillus fumigatus* mutant reveals involvement of the Tor kinase in iron
796 regulation. Proteomics. 2015; 15(13): 2230-43.
797 [31] Teichert S, Wottawa M, Schönig B, et al. Role of the *Fusarium fujikuroi* TOR
798 kinase in nitrogen regulation and secondary metabolism. Eukaryot Cell. 2006;
799 5(10): 1807-19.
800 [32] Meléndez HG, Billon-Grand G, Fèvre M, et al. Role of the *Botrytis cinerea*
801 FKBP12 ortholog in pathogenic development and in sulfur regulation. Fungal
802 Genet Biol. 2009; 46(4): 308-20.
803 [33] López-Berges MS, Rispail N, Prados-Rosales RC, et al. A nitrogen response
804 pathway regulates virulence functions in *Fusarium oxysporum* via the protein
805 kinase TOR and the bZIP protein MeaB. Plant Cell. 2010; 22(7): 2459-75.
806 [34] Bastidas RJ, Shertz CA, Lee SC, et al. Rapamycin exerts antifungal activity *in*
807 *vitro* and *in vivo* against *Mucor circinelloides* via FKBP12-dependent inhibition
808 of Tor. Eukaryot Cell. 2012; 11(3): 270-81.

809 [35] Madrid, M, Vázquez-Marín, B, Franco, A, et al. Multiple crosstalk between TOR
810 and the cell integrity MAPK signaling pathway in fission yeast. Sci Rep. 2016
811 Nov 23; 6: 37515.
812 [36] Torres J, Di Como CJ, Herrero E, et al. Regulation of the cell integrity pathway
813 by rapamycin-sensitive TOR function in budding yeast. J Biol Chem. 2002 Nov 8;
814 277(45): 43495-504.
815 [37] Chen DD, Shi L, Yue SN, et al. The Slt2-MAPK pathway is involved in the
816 mechanism by which target of rapamycin regulates cell wall components in
817 *Ganoderma lucidum*. Fungal Genet Biol. 2019; 123: 70-77.
818 [38] Gu Q, Zhang C, Yu F, et al. Protein kinase FgSch9 serves as a mediator of the
819 target of rapamycin and high osmolarity glycerol pathways and regulates multiple
820 stress responses and secondary metabolism in *Fusarium graminearum*. Environ
821 Microbiol. 2015; 17(8): 2661-76.
822 [39] Qian B, Liu X, Jia J, et al. MoPpe1 partners with MoSap1 to mediate TOR and
823 cell wall integrity signalling in growth and pathogenicity of the rice blast fungus
824 *Magnaporthe oryzae*. Environ Microbiol. 2018; 20(11): 3964-3979.
825 [40] Qian B, Liu X, Ye Z, et al. Phosphatase-associated protein MoTip41 interacts
826 with the phosphatase MoPpe1 to mediate crosstalk between TOR and cell wall
827 integrity signalling during infection by the rice blast fungus *Magnaporthe oryzae*.
828 Environ Microbiol. 2021; 23(2): 791-809.
829 [41] Tong M, Jiang Y. FK506-binding proteins and their diverse functions. Curr Mol
830 Pharmacol. 2015; 9(1): 48-65.

831 [42] Heitman J, Movva NR, Hall MN. Targets for cell cycle arrest by the
832 immunosuppressant rapamycin in yeast. Science. 1991; 253(5022): 905-9.
833 [43] Ren S, Yang M, Yue Y, et al. Lysine succinylation contributes to aflatoxin
834 production and pathogenicity in *Aspergillus flavus*. Mol Cell Proteomics. 2018;
835 17(3): 457-471.
836 [44] Weisman R. Target of rapamycin (TOR) regulates growth in response to
837 nutritional signals. Microbiol Spectr. 2016; 4(5).
838 [45] Loewith R, Hall MN. Target of rapamycin (TOR) in nutrient signaling and
839 growth control. Genetics. 2011; 189(4): 1177-201.
840 [46] Pascual-Ahuir A, Proft M. The Sch9 kinase is a chromatin-associated
841 transcriptional activator of osmostress-responsive genes. EMBO J. 2007; 26(13):
842 3098-108.
843 [47] Düvel K, Broach JR. The role of phosphatases in TOR signaling in yeast. Curr
844 Top Microbiol Immunol. 2004; 279: 19-38.
845 [48] Jacinto E, Guo B, Arndt KT, et al. TIP41 interacts with TAP42 and negatively
846 regulates the TOR signaling pathway. Mol Cell. 2001; 8(5): 1017-26.
847 [49] Sánchez-Álvarez M, Del Pozo MÁ, Bosch M, et al. Insights into the biogenesis
848 and emerging functions of lipid droplets from unbiased molecular profiling
849 approaches. Front Cell Dev Biol. 2022; 10: 901321.
850 [50] Gizachew D, Chang CH, Szonyi B, et al. Aflatoxin B1 (AFB_1) production by
851 *Aspergillus flavus* and *Aspergillus parasiticus* on ground Nyjer seeds: the effect
852 of water activity and temperature. Int J Food Microbiol. 2019; 296: 8-13.

853 [51] Cruz MC, Goldstein AL, Blankenship J, et al. Rapamycin and less
854 immunosuppressive analogs are toxic to *Candida albicans* and *Cryptococcus*
855 *neoformans* via FKBP12-dependent inhibition of TOR. Antimicrob Agents
856 Chemother. 2001; 45(11): 3162-70.
857 [52] Galat A. Functional diversity and pharmacological profiles of the FKBPs and
858 their complexes with small natural ligands. Cell Mol Life Sci. 2013; 70(18):
859 3243-75.
860 [53] Kasahara K. Physiological function of FKBP12, a primary target of
861 rapamycin/FK506: a newly identified role in transcription of ribosomal protein
862 genes in yeast. Curr Genet. 2021 Jun; 67(3): 383-388.
863 [54] Li Y, Ren H, Zhao Y, et al. Characterization of three FK506-binding proteins in
864 the entomopathogenic fungus *Beauveria bassiana*. J Invertebr Pathol. 2020; 171:
865 107334.
866 [55] Xiong Y, Sheen J. The role of target of rapamycin signaling networks in plant
867 growth and metabolism. Plant Physiol. 2014; 164(2): 499-512.
868 [56] Adami A, García-Alvarez B, Arias-Palomo E, et al. Structure of TOR and its
869 complex with KOG1. Mol Cell. 2007; 27(3): 509-16.
870 [57] Tatebe H, Shiozaki K. Evolutionary conservation of the components in the TOR
871 signaling pathways. Biomolecules. 2017 ;7(4):77.
872 [58] Ma YC, Dai LL, Qiu BB, et al. TOR functions as a molecular switch connecting
873 an iron cue with host innate defense against bacterial infection. PLoS Genet. 2021;
874 17(3): e1009383.

875 [59] Baldin C, Valiante V, Krüger T, et al. Comparative proteomics of a tor inducible
876 *Aspergillus fumigatus* mutant reveals involvement of the Tor kinase in iron
877 regulation. Proteomics. 2015; 15(13): 2230-43.
878 [60] Jiang Y, Broach JR. Tor proteins and protein phosphatase 2A reciprocally regulate
879 Tap42 in controlling cell growth in yeast. EMBO J. 1999;18(10):2782-92.
880 [61] Fenyvuesvolgyi C, Elder RT, Benko Z, et al. Fission yeast homologue of
881 Tip41-like proteins regulates type 2A phosphatases and responses to nitrogen
882 sources. Biochim Biophys Acta. 2005; 1746(2): 155-62.
883 [62] Nakashima A, Tanimura-Ito K, Oshiro N, et al. A positive role of mammalian
884 Tip41-like protein, TIPRL, in the amino-acid dependent mTORC1-signaling
885 pathway through interaction with PP2A. FEBS Lett. 2013; 587(18): 2924-9.
886 [63] Han Q, Pan C, Wang Y, et al. PP2A-like protein phosphatase (Sit4) regulatory
887 subunits, Sap155 and Sap190, regulate *Candida albicans*' cell growth,
888 morphogenesis, and virulence. Front Microbiol. 2019; 10: 2943.
889 [64] Tan L, Chen H, Yu S, et al. A SOE-PCR method of introducing multiple
890 mutations into Mycoplasma gallisepticum neuraminidase. J Microbiol Methods.
891 2013; 94(2): 117-120.
892 [65] Zadra I, Abt B, Parson W, Haas H. *xylP* promoter-based expression system and its
893 use for antisense downregulation of the *Penicillium chrysogenum* nitrogen
894 regulator NRE. Appl Environ Microbiol. 2000;66(11):4810-6.
895 [66] Nie X, Yu S, Qiu M, et al. *Aspergillus flavus* SUMO contributes to fungal
896 virulence and toxin attributes. J Agric Food Chem. 2016 Sep 7; 64(35): 6772-82.

[67] Tan C, Deng J, Zhang F, et al. CWI pathway participated in vegetative growth and pathogenicity through a downstream effector AflRlm1 in *Aspergillus flavus*. iScience. 2021;24(10):103159.

[68] Livak KJ, Schmittgen TD. Analysis of relative gene expression data using real-time quantitative PCR and the $2^{-\Delta\Delta CT}$ method. Methods. 2001; 25(4): 402–408.

[69] Chang PK, Scharfenstein LL, Wei Q, Bhatnagar D. Development and refinement of a high-efficiency gene-targeting system for *Aspergillus flavus*. J Microbiol Methods. 2010;81(3):240-6.

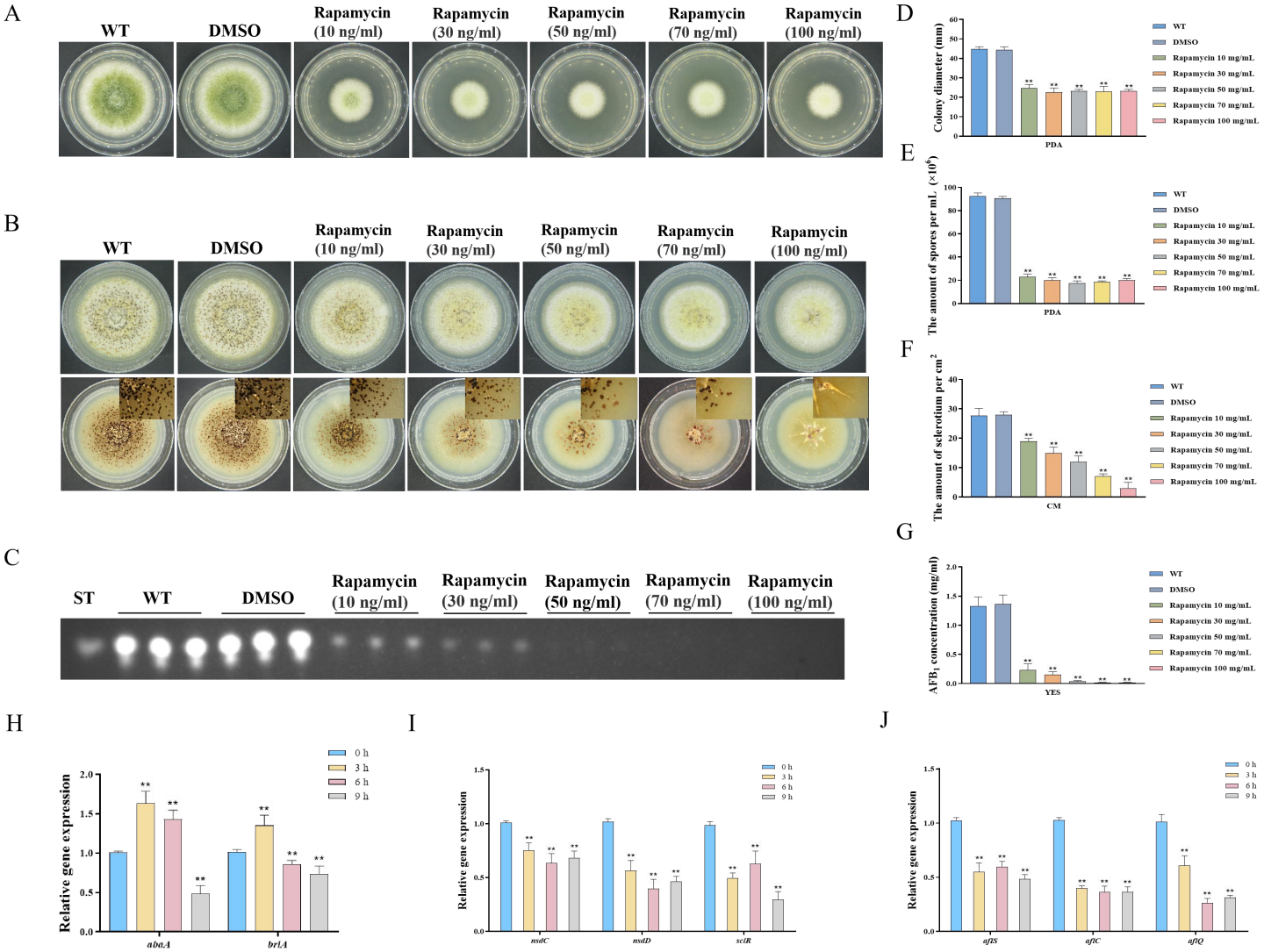
A
WT
DMSO
Rapamycin (10 ng/ml)
Rapamycin (30 ng/ml)
Rapamycin (50 ng/ml)
Rapamycin (70 ng/ml)
Rapamycin (100 ng/ml)
B
C
ST
D
Colony diameter (mm)
PDA
E
The amount of spores per mL (×10^6)
F
The amount of sclerotium per cm^2
CM
G
AFB1 concentration (mg/ml)
YES
Rapamycin 10 mg/mL
Rapamycin 30 mg/mL
Rapamycin 50 mg/mL
Rapamycin 70 mg/mL
Rapamycin 100 mg/mL
H
Relative gene expression
0 h
3 h
6 h
9 h
abaA
brlA
I
nsdC
nsdD
sclR
J
aflS
aflC
aflQ

Fig. 1 Impacts of rapamycin on the growth, sporulation, sclerotia formation,and aflatoxin production of *Aspergillus flavus*.

(A) Colony morphology of the WT strain cultured on PDA medium amended with different concentrations of rapamycin at 37°C for 5 days.

(B) Colony phenotype of the WT strain grown on CM medium amended with different concentrations of rapamycin at 37°C for 7 days.

(C) TLC assay of AFB_1 production by the WT strain cultured in YES liquid media amended with different concentrations of rapamycin at 29°C for 6 days.

(D) Statistical analysis of the colony diameter by the WT strain treated with different concentrations of rapamycin described in (A).

(E) Conidial quantification of the WT strain treated with different concentrations of rapamycin as mentioned in (A).

(F) Quantitative analysis of sclerotium formation by the WT strain treated with different concentrations of rapamycin described in (B).

(G) Relative quantification of AFB_1 production by the WT strain treated with different concentrations of rapamycin as mentioned in (C)

(H) Relative expression levels of conidia-related genes in WT strain treated with 100 ng/mL rapamycin after 3, 6, 9 h.

(I) Relative expression levels of sclerotia-related genes in WT strain treated with 100 ng/mL rapamycin after 3, 6, 9 h.

(J) Relative expression levels of aflatoxin biosynthesis regulatory and structural genes in WT strain treated with 100 ng/mL rapamycin after 3, 6, 9 h.

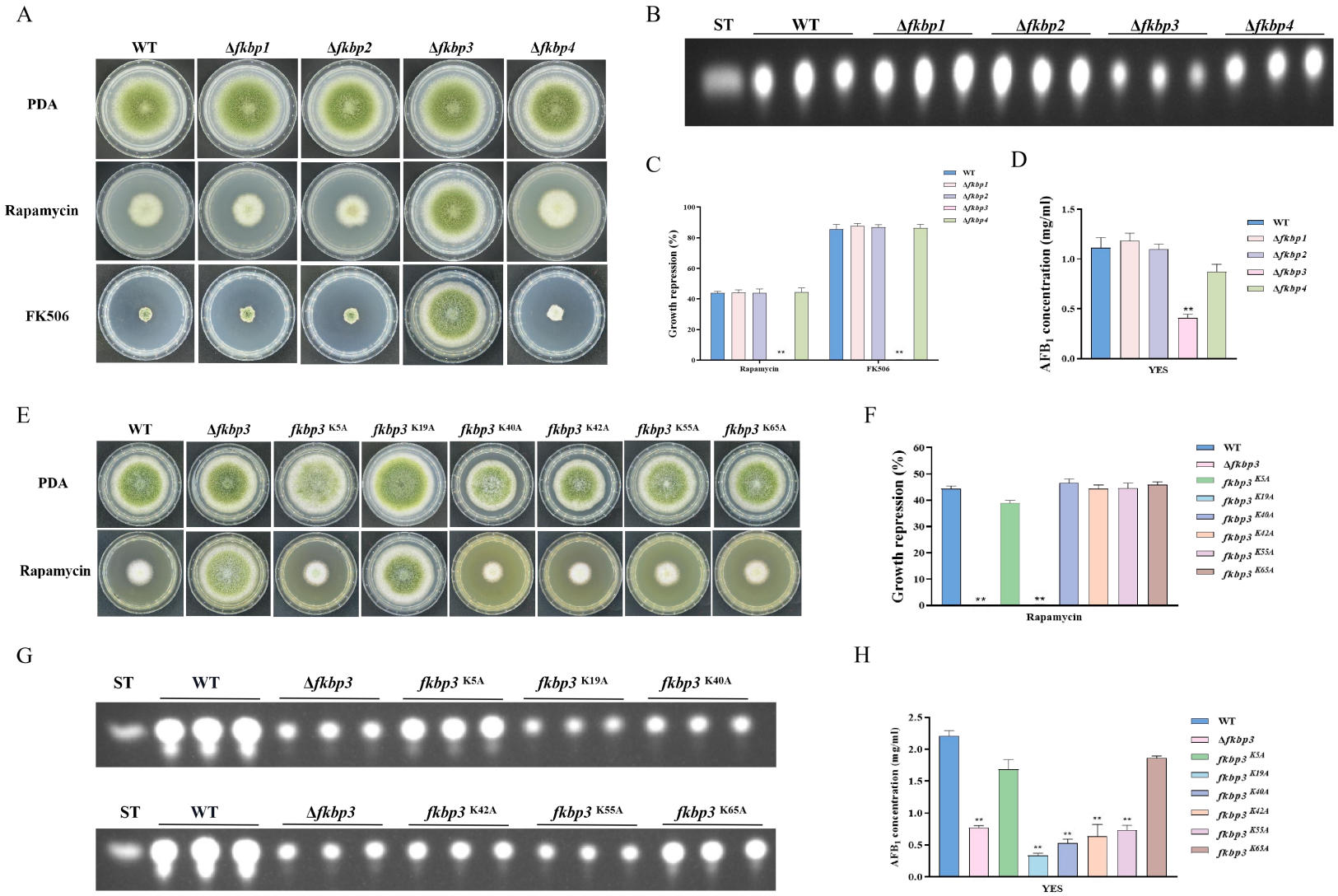
A
WT
Δfkbp1
Δfkbp2
Δfkbp3
Δfkbp4
PDA
Rapamycin
FK506
B
ST
WT
Δfkbp1
Δfkbp2
Δfkbp3
Δfkbp4
C
Growth repression (%)
Rapamycin
FK506
D
AFB1 concentration (mg/ml)
YES
E
WT
Δfkbp3
fkbp3 K5A
fkbp3 K19A
fkbp3 K40A
fkbp3 K42A
fkbp3 K55A
fkbp3 K65A
PDA
Rapamycin
F
Growth repression (%)
Rapamycin
G
ST
WT
Δfkbp3
fkbp3 K5A
fkbp3 K19A
fkbp3 K40A
fkbp3 K42A
fkbp3 K55A
fkbp3 K65A
H
AFB1 concentration (mg/ml)
YES

Fig. 2 Disruption of *fkbp3* significantly increases the resistance of *A. flavus* to rapamycin and FK506.

(A) Phenotype of the WT and all mutant strains (Δ*fkbp1*, Δ*fkbp2*, Δ*fkbp3*, and Δ*fkbp4*) grown on PDA amended with rapamycin and FK506 at 37°C for 5 days.

(B) TLC analysis of AFB_1 production by the WT and all mutant strains (Δ*fkbp1*, Δ*fkbp2*, Δ*fkbp3*, and Δ*fkbp4*) cultured in YES liquid medium at 29°C for 6 days.

(C) The growth inhibition rate of the WT and all mutant strains (Δ*fkbp1*, Δ*fkbp2*, Δ*fkbp3*, and Δ*fkbp4*) under rapamycin and FK506 stress.

(D) AFB_1 quantitative analysis of the WT and all mutant strains (Δ*fkbp1*, Δ*fkbp2*, Δ*fkbp3*, and Δ*fkbp4*) as described in (B).

(E) Phenotype of the WT and all mutant strains (Δ*fkbp3*, K5A, K19A, K40A, K42A, K55A, and K65A) grown on PDA amended with 100 ng/mL rapamycin at 37°C for 5 days.

(F) The growth inhibition rate of the WT and all mutant strains (Δ*fkbp3*, K5A, K19A, K40A, K42A, K55A, and K65A) under rapamycin stress.

(G) TLC assay of AFB_1 production by the WT and all mutant strains (Δ*fkbp3*, K5A, K19A, K40A, K42A, K55A, and K65A) cultured in YES liquid medium at 29°C for 6 days.

(H) Relative quantification of AFB_1 production in the WT and all mutant strains (Δ*fkbp3*, K5A, K19A, K40A, K42A, K55A, and K65A) as mentioned in (G).

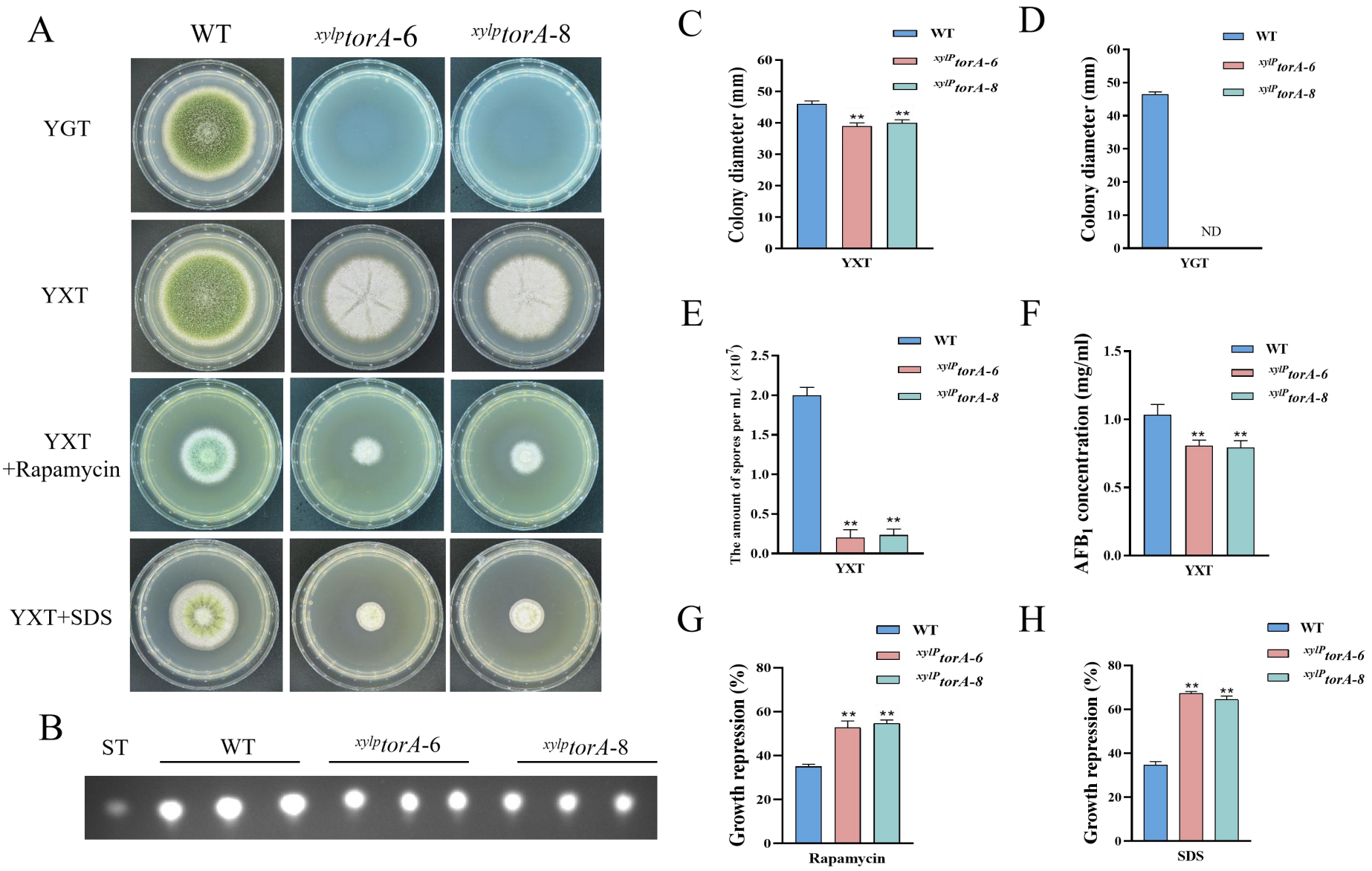
A
WT
xylptorA-6
xylptorA-8
YGT
YXT
YXT
+Rapamycin
YXT+SDS
B
ST
WT
xylptorA-6
xylptorA-8
C
Colony diameter (mm)
YXT
D
Colony diameter (mm)
ND
YGT
E
The amount of spores per mL (×10^7)
YXT
F
AFB1 concentration (mg/ml)
YXT
G
Growth repression (%)
Rapamycin
H
Growth repression (%)
SDS
WT
xylPtorA-6
xylPtorA-8

Fig. 3 The TorA kinase plays a critical role in *A. flavus*

(A) Phenotype of the WT and the ^{xylP}*torA* strains in YGT and YXT medium amended with 100 ng/mL rapamycin and 300 mg/mL SDS at 37°C for 5 days.

(B) TLC assay of AFB_1 production from the WT and the ^{xylP}*torA* strains cultured in s on YXT medium containing 1 g/L $MgSO_4 \cdot 7H_2O$ at 29°C for 6 days.

(C) Statistical analysis of the colony diameter by the WT and the ^{xylP}*torA* strains in YXT medium.

(D) Statistical analysis of the colony diameter by the WT and the ^{xylP}*torA* strains in YGT medium.

(E) Conidial quantification of theWT and the ^{xylP}*torA* strains in YXT medium.

(F) Quantitative analysis of AFB_1 as shown in (B).

(G) The growth inhibition rate of the WT and the ^{xylP}*torA* strains under rapamycin.

(H) The growth inhibition rate of the WT and the ^{xylP}*torA* strains under SDS stress.

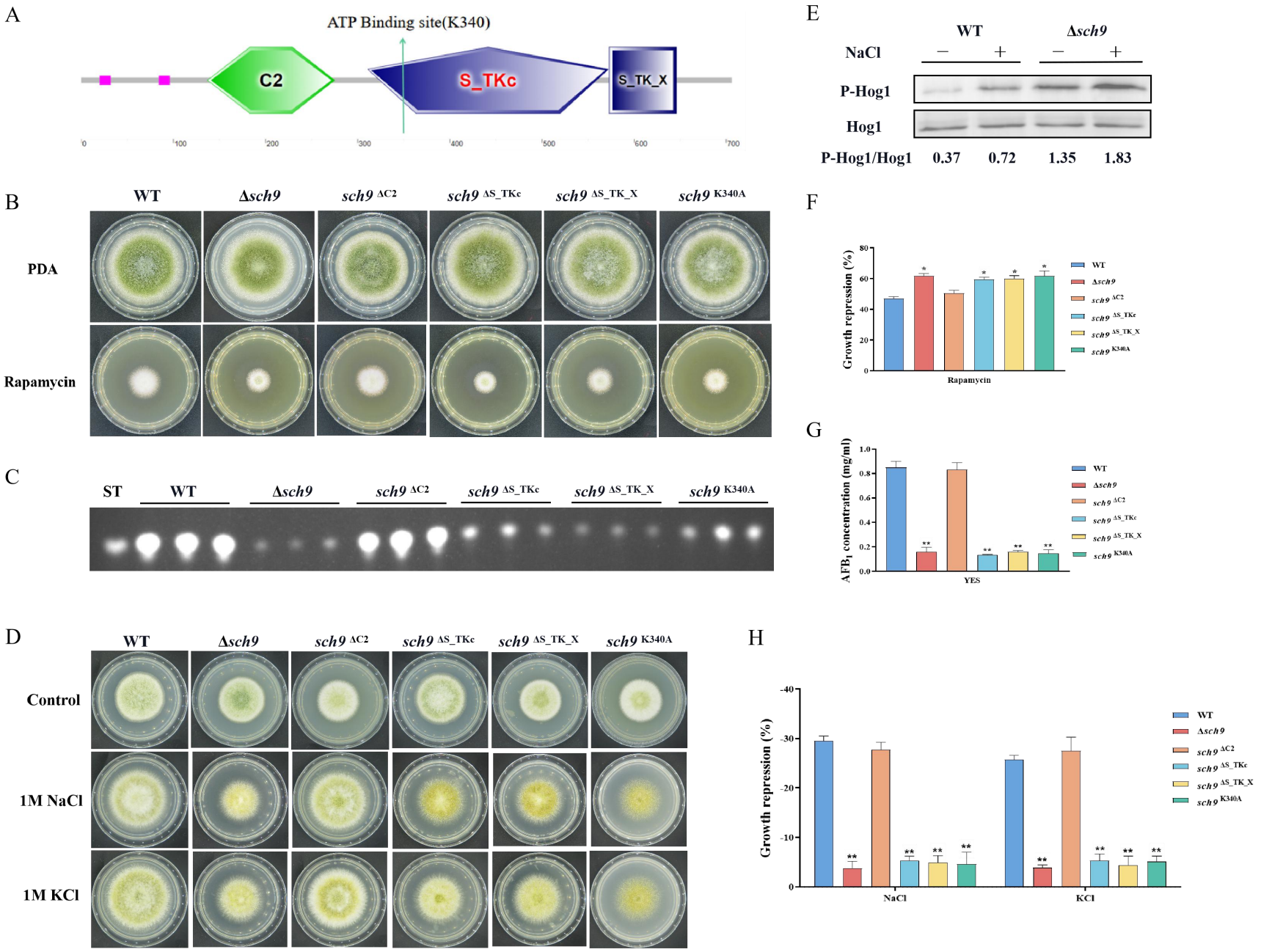
A
ATP Binding site(K340)
C2
S_TKc
S_TK_X
0
100
200
300
400
500
600
700
B
WT
Δsch9
sch9 ΔC2
sch9 ΔS_TKc
sch9 ΔS_TK_X
sch9 K340A
PDA
Rapamycin
C
ST
WT
Δsch9
sch9 ΔC2
sch9 ΔS_TKc
sch9 ΔS_TK_X
sch9 K340A
D
WT
Δsch9
sch9 ΔC2
sch9 ΔS_TKc
sch9 ΔS_TK_X
sch9 K340A
Control
1M NaCl
1M KCl
E
WT
Δsch9
NaCl
−
+
−
+
P-Hog1
Hog1
P-Hog1/Hog1
0.37
0.72
1.35
1.83
F
Growth repression (%)
80
60
40
20
0
Rapamycin
WT
Δsch9
sch9 ΔC2
sch9 ΔS_TKc
sch9 ΔS_TK_X
sch9 K340A
G
AFB1 concentration (mg/ml)
1.0
0.8
0.6
0.4
0.2
0.0
YES
WT
Δsch9
sch9 ΔC2
sch9 ΔS_TKc
sch9 ΔS_TK_X
sch9 K340A
H
Growth repression (%)
-40
-30
-20
-10
0
NaCl
KCl
WT
Δsch9
sch9 ΔC2
sch9 ΔS_TKc
sch9 ΔS_TK_X
sch9 K340A

Fig. 4 The Sch9 kinase participates in aflatoxin biosynthesis and the HOG pathway.

(A) The structure diagram of the Sch9 kinase.

(B) Phenotype of the WT, Δ*sch9*, *sch9*$^{\Delta C2}$, *sch9*$^{\Delta S_TKc}$, *sch9*$^{\Delta S_TK_X}$, and *sch9*^{K340A} strains grown on PDA medium amended with 100 ng/mL rapamycin at 37°C for 5 days.

(C) TLC assay of AFB_1 production from the WT, Δ*sch9*, *sch9*$^{\Delta C2}$, *sch9*$^{\Delta S_TKc}$, *sch9*$^{\Delta S_TK_X}$, and *sch9*^{K340A} strains cultured in YES liquid medium at 29°C for 6 days.

(D) The phenotypes of the WT, Δ*sch9*, *sch9*$^{\Delta C2}$, *sch9*$^{\Delta S_TKc}$, *sch9*$^{\Delta S_TK_X}$, and *sch9*^{K340A}strains on YGT media amended with 1 M NaCl and 1 M KCl for 3 days.

(E) The phosphorylation levels of Hog1 in the WT and Δ*sch9* strains were determined with or without osmotic stress.

(F) The growth inhibition rate of the WT, Δ*sch9*, *sch9*$^{\Delta C2}$, *sch9*$^{\Delta S_TKc}$, *sch9*$^{\Delta S_TK_X}$, and *sch9*^{K340A} strains under rapamycin stress.

(G) Quantitative analysis of AFB_1 as shown in (C).

(H) The growth inhibition rate of the WT, Δ*sch9*, *sch9*$^{\Delta C2}$, *sch9*$^{\Delta S_TKc}$, *sch9*$^{\Delta S_TK_X}$, and *sch9*^{K340A} strains under osmotic stress.

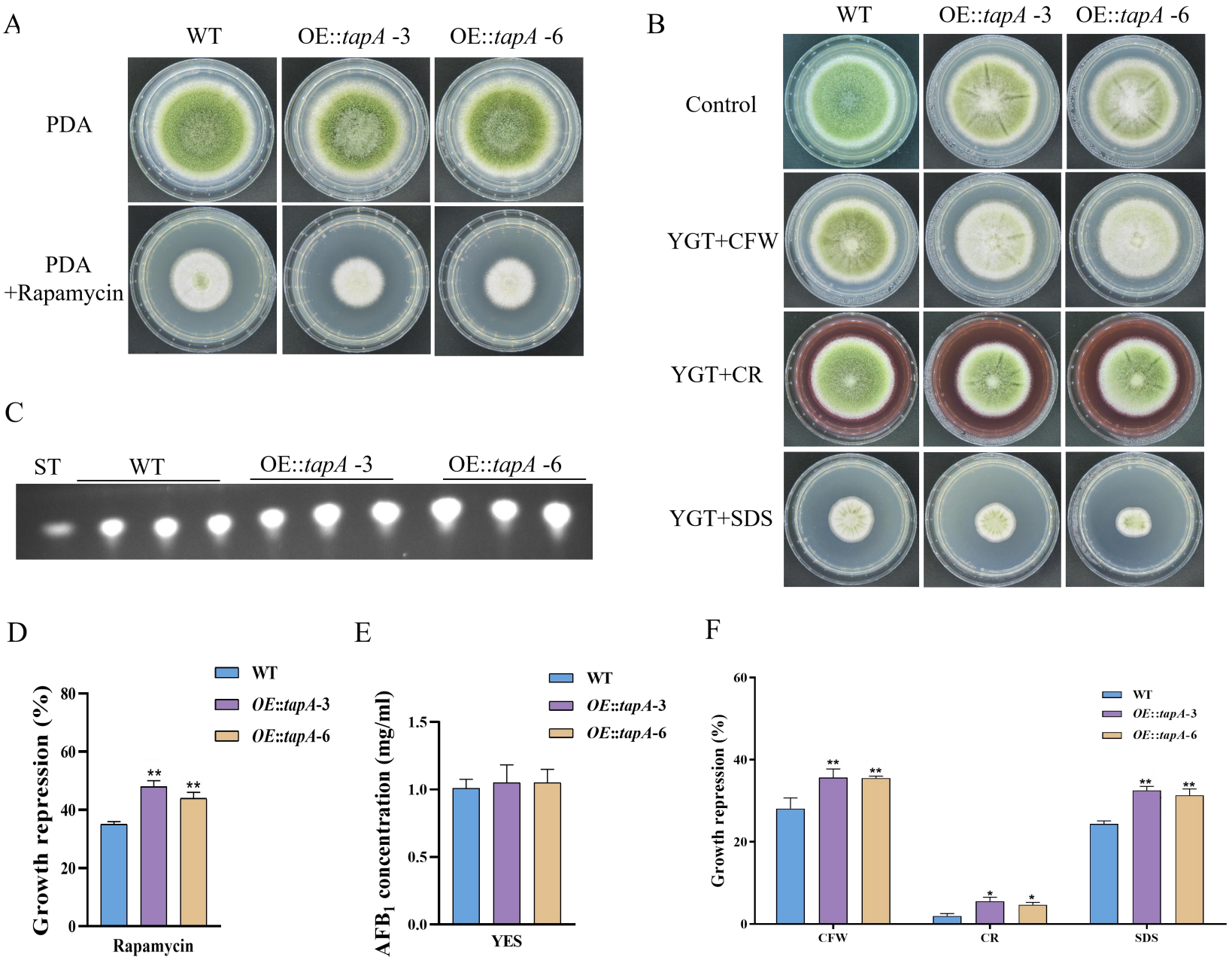
A
WT
OE::tapA -3
OE::tapA -6
PDA
PDA
+Rapamycin
B
WT
OE::tapA -3
OE::tapA -6
Control
YGT+CFW
YGT+CR
YGT+SDS
C
ST
WT
OE::tapA -3
OE::tapA -6
D
Growth repression (%)
WT
OE::tapA-3
OE::tapA-6
Rapamycin
E
AFB1 concentration (mg/ml)
WT
OE::tapA-3
OE::tapA-6
YES
F
Growth repression (%)
WT
OE::tapA-3
OE::tapA-6
CFW
CR
SDS

Fig. 5 TapA regulates cell wall stress in *A. flavus.*

(A) Phenotype of the WT and *OE*::*tapA* strains grown on PDA amended with 100 ng/mL rapamycin at 37°C for 5 days.

(B) Colony morphology of the WT and *OE*::*tapA* strains grown on PDA media supplemented with 200 μg/mL CR, 200μg/mL CFW, or 300 μg/mL SDS at 37°C for 5 days.

(C) TLC assay of AFB_1 production by the WT and *OE*::*tapA* strains cultured in YES liquid medium at 29°C for 6 days.

(D) The growth inhibition rate of the WT and *OE*::*tapA* strains under rapamycin.

(E) Quantitative analysis of AFB_1 as shown in (C).

(F) The growth inhibition rate of the WT and *OE*::*tapA* strains under cell wall and cell membrane stress.

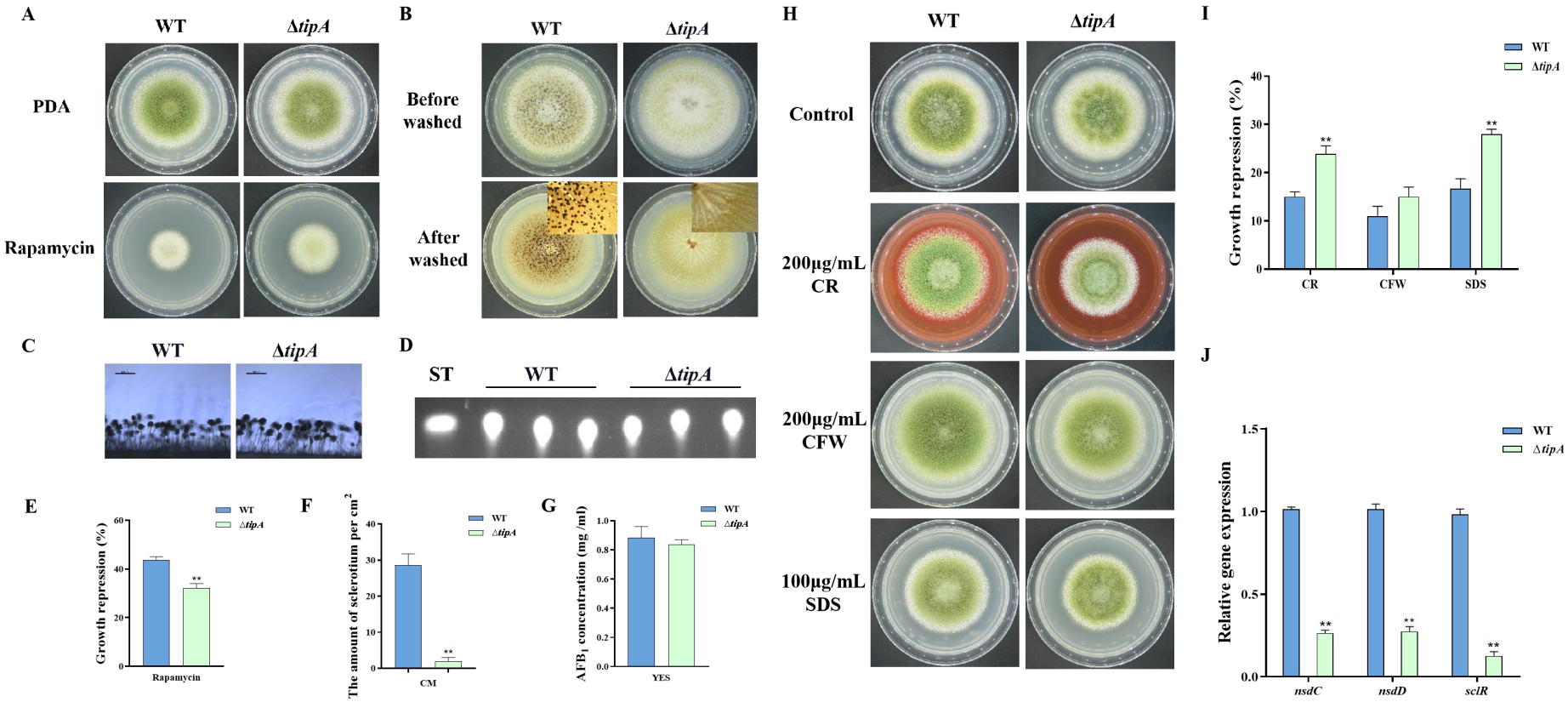
A
WT
ΔtipA
PDA
Rapamycin
B
WT
ΔtipA
Before washed
After washed
C
WT
ΔtipA
D
ST
WT
ΔtipA
E
Growth repression (%)
WT
ΔtipA
Rapamycin
F
The amount of sclerotium per cm2
WT
ΔtipA
CM
G
AFB1 concentration (mg /ml)
WT
ΔtipA
YES
H
WT
ΔtipA
Control
200μg/mL CR
200μg/mL CFW
100μg/mL SDS
I
Growth repression (%)
WT
ΔtipA
CR
CFW
SDS
J
Relative gene expression
WT
ΔtipA
nsdC
nsdD
sclR

Fig. 6 TipA regulates sclerotia development and cell wall stress in *A. flavus.*

(A) Phenotype of the WT and Δ*tipA* strains grown on PDA amended with 100 ng/mL rapamycin at 37°C for 5 days.

(B) Phenotypic characterization of the WT and Δ*tipA* strains grown on CM medium at 37°C for 7 days.

(C) Morphology of conidiophores in the WT and Δ*tipA* strains observed by microscope.

(D) TLC assay of AFB_1 production by the WT and Δ*tipA* strains cultured in YES liquid medium at 29°C for 6 days.

(E) The growth inhibition rate of the WT and Δ*tipA* strains under rapamycin stress.

(F) Amount of sclerotia produced by the WT and Δ*tipA* strains.

(G) AFB_1 quantitative analysis of the WT and Δ*tipA* strains described in (D).

(H) Colony morphology of the WT and Δ*tipA* strains grown on PDA media supplemented with 200 μg/mL CR, 200μg/mL CFW, and 100 μg/mLSDS at 37°C for 5 days.

(I) The growth inhibition rate of the WT and Δ*tipA* strains under cell wall and cell membrane stress.

(J) Relative expression levels of sclerotia formation genes in the WT and Δ*tipA* strains.

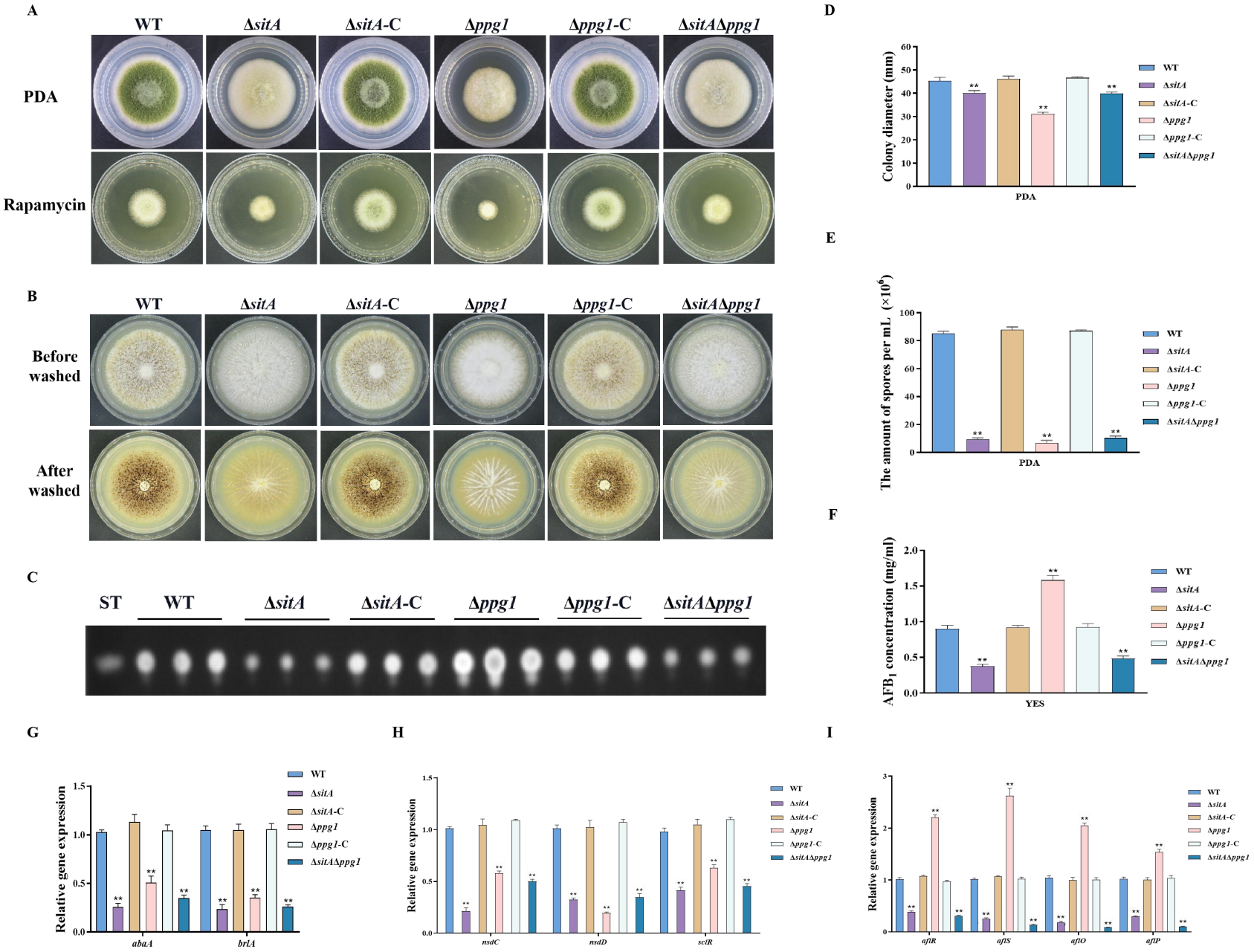
A
WT
ΔsitA
ΔsitA-C
Δppg1
Δppg1-C
ΔsitAΔppg1
PDA
Rapamycin
B
Before washed
After washed
C
ST
D
Colony diameter (mm)
PDA
E
The amount of spores per mL (×10^6)
F
AFB1 concentration (mg/ml)
YES
G
Relative gene expression
abaA
brlA
H
nsdC
nsdD
sclR
I
aflR
aflS
aflO
aflP

Fig. 7 The impact of the phosphatases SitA and Ppg1 on the growth, conidiation, and aflatoxin biosynthesis in *A. flavus*.

(A) Colony morphology of the WT, single knockout, and double knockout strains cultured on PDA medium amended with 100 ng/mL rapamycin at 37℃ for 5 days.

(B) Colony morphology of the WT, single knockout, and double knockout strains cultured on CM medium at 37℃ for 7 days.

(C) TLC analysis of AFB_1 production from the WT, single knockout, and double knockout strains cultured in YES liquid medium at 29℃ for 6 days.

(D) Growth diameter of the WT, single knockout, and double knockout strains on PDA media.

(E) The growth inhibition rate of the WT, single knockout, and double knockout strains under rapamycin stress.

(F) AFB_1 quantitative analysis of the WT, single knockout, and double knockout strains.

(G) Relative expression levels of conidia synthesis genes in the WT, single knockout, and double knockout strains.

(H) Relative expression levels of sclerotia synthesis genes in the WT, single knockout, and double knockout strains.

(I) Relative expression levels of aflatoxin biosynthesis genes in the WT, single knockout, and double knockout strains.

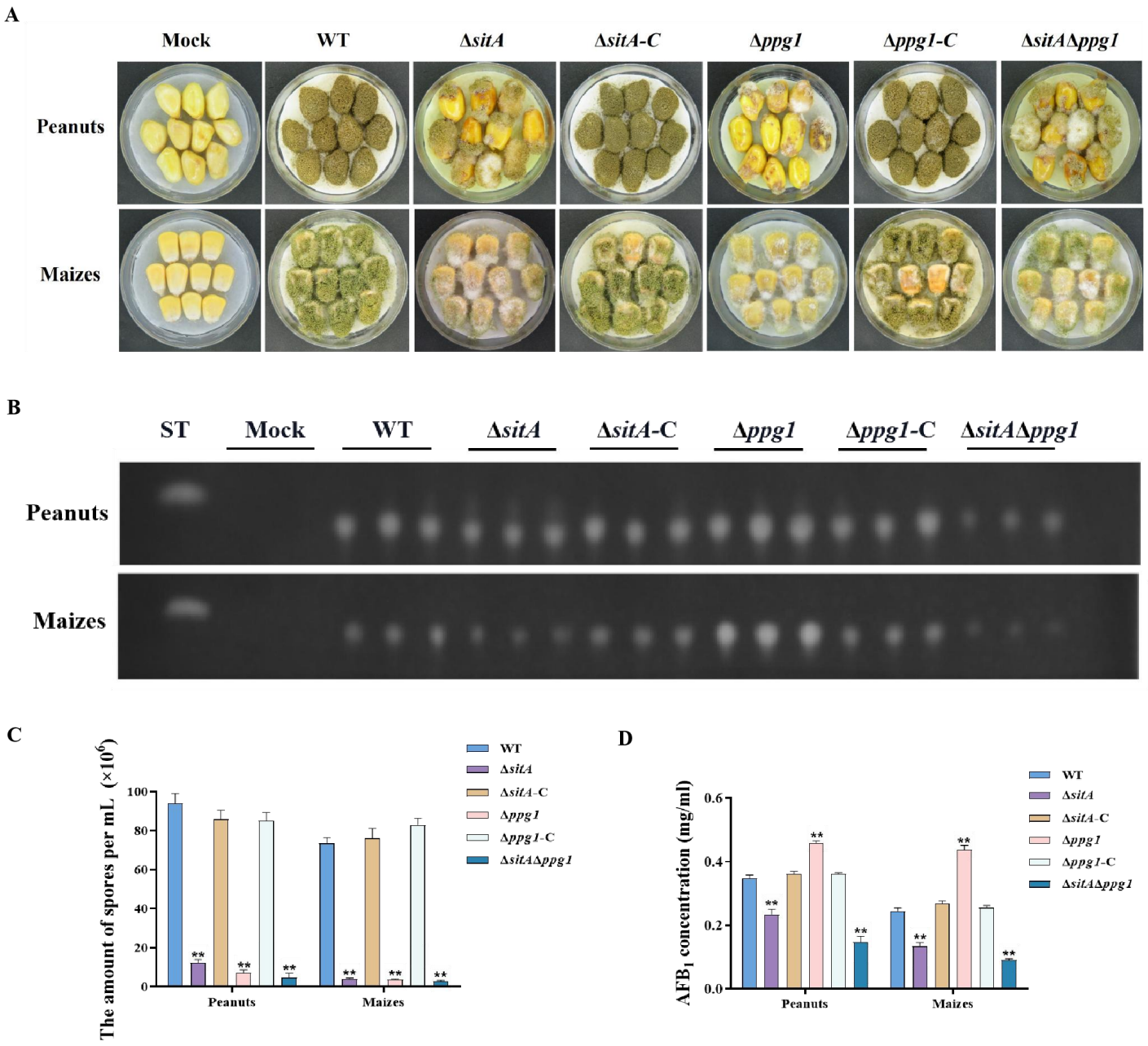
A
Mock
WT
ΔsitA
ΔsitA-C
Δppg1
Δppg1-C
ΔsitAΔppg1
Peanuts
Maizes
B
ST
Mock
WT
ΔsitA
ΔsitA-C
Δppg1
Δppg1-C
ΔsitAΔppg1
Peanuts
Maizes
C
The amount of spores per mL (×10^6)
100
80
60
40
20
0
Peanuts
Maizes
WT
ΔsitA
ΔsitA-C
Δppg1
Δppg1-C
ΔsitAΔppg1
D
AFB1 concentration (mg/ml)
0.6
0.4
0.2
0.0
Peanuts
Maizes
WT
ΔsitA
ΔsitA-C
Δppg1
Δppg1-C
ΔsitAΔppg1

Fig. 8 Pathogenicity analysis of the phosphatase SitA and Ppg1 in *A. flavus*.

(A) Phenotypes of peanut and maize infected by the WT, single knockout, and double knockout strains.

(B) TLC was used to detect the AFB_1 from peanut and maize infected by the WT, single knockout, and double knockout strains.

(C) Quantitative analysis of conidia production from peanut and maize infected by the WT, single knockout, and double knockout strains.

(D) Quantitative analysis of AFB_1 from peanut and maize infected by the WT, single knockout, and double knockout strains.

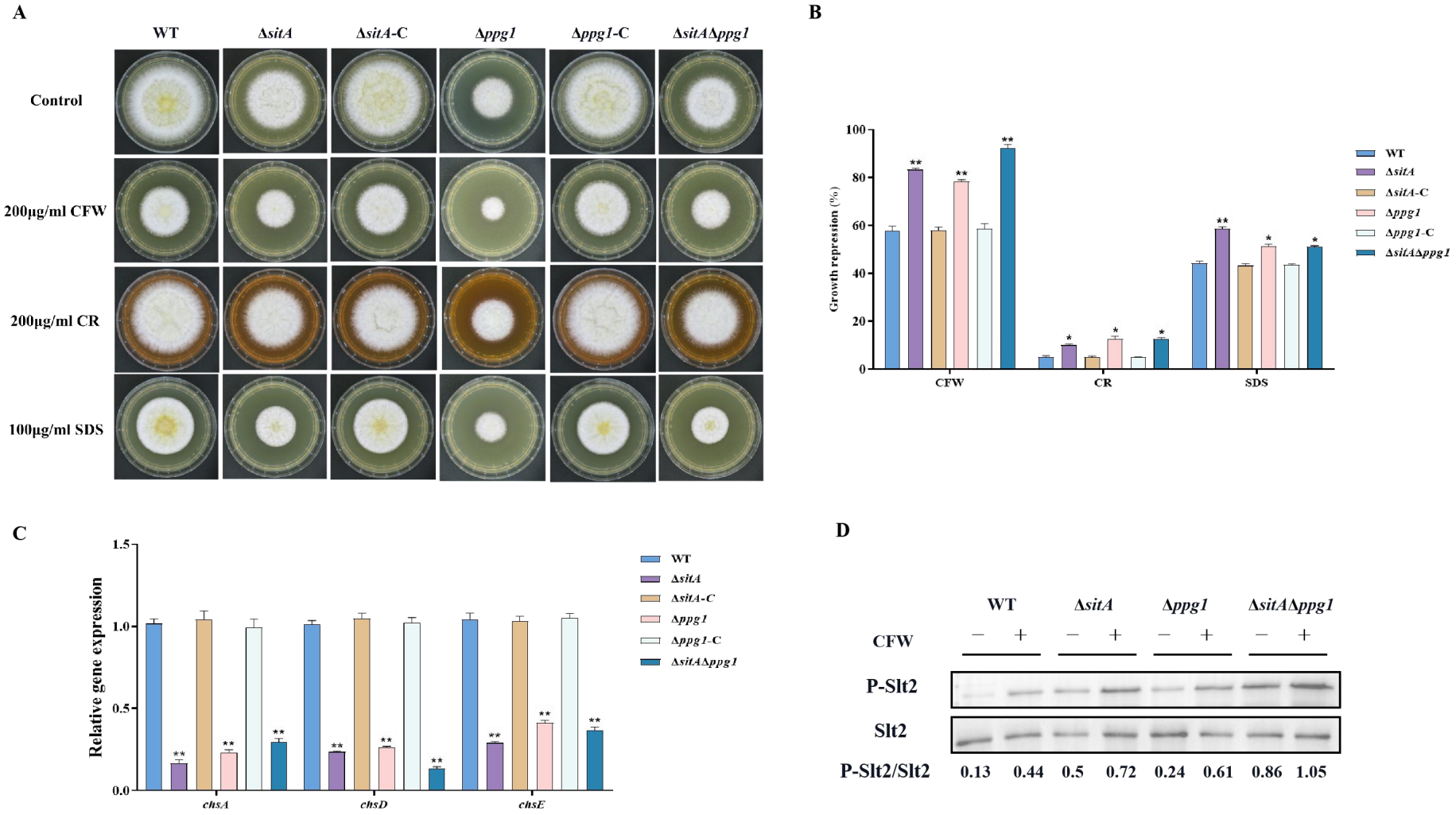
A
WT
ΔsitA
ΔsitA-C
Δppg1
Δppg1-C
ΔsitAΔppg1
Control
200μg/ml CFW
200μg/ml CR
100μg/ml SDS
B
Growth repression (%)
100
80
60
40
20
0
CFW
CR
SDS
WT
ΔsitA
ΔsitA-C
Δppg1
Δppg1-C
ΔsitAΔppg1
C
Relative gene expression
1.5
1.0
0.5
0.0
chsA
chsD
chsE
WT
ΔsitA
ΔsitA-C
Δppg1
Δppg1-C
ΔsitAΔppg1
D
WT
ΔsitA
Δppg1
ΔsitAΔppg1
CFW
− + − + − + − +
P-Slt2
Slt2
P-Slt2/Slt2
0.13 0.44 0.5 0.72 0.24 0.61 0.86 1.05

Fig. 9 Sensitivity of phosphatase SitA and Ppg1 to cell wall damaging agents in *A. flavus*.

(A) Morphology of the WT, single knockout, and double knockout strains grown on YES media supplemented with 200 μg/mL CR, 200 μg/mL CFW, or 100 μg/mL SDS at 37°C for 5 days.

(B) The growth inhibition rate of the WT, single knockout, and double knockout strains under cell wall and cell membrane stress.

(C) Relative expression levels of cell wall synthesis genes (*chsA*, *chsD* and *chsE*) in the WT, single knockout, and double knockout strains.

(D) The phosphorylation level of Slt2 in the WT, single knockout, and double knockout strains was detected with or without cell wall stress.

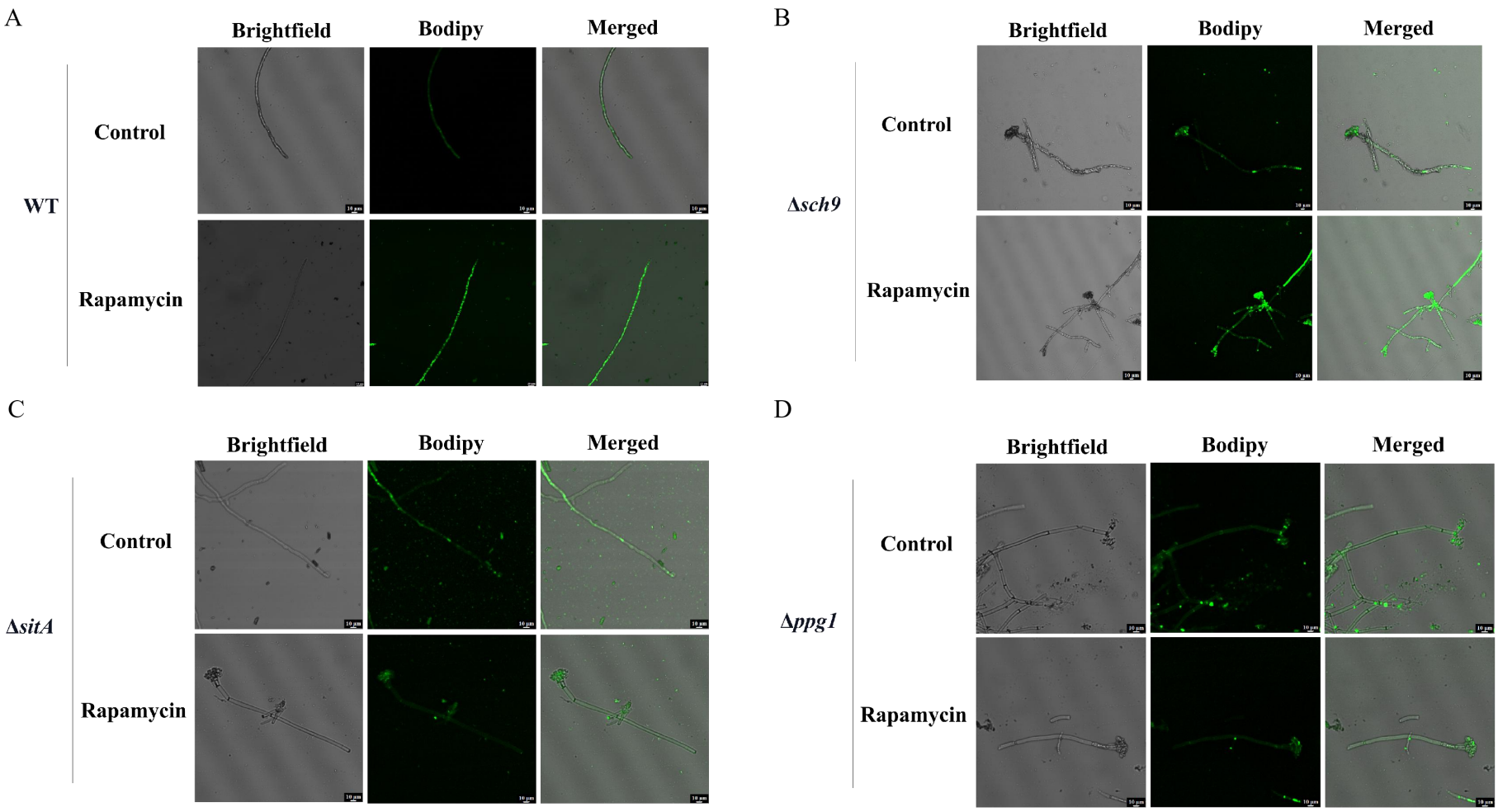
A
Brightfield
Bodipy
Merged
WT
Control
Rapamycin
B
Brightfield
Bodipy
Merged
Δsch9
Control
Rapamycin
C
Brightfield
Bodipy
Merged
ΔsitA
Control
Rapamycin
D
Brightfield
Bodipy
Merged
Δppg1
Control
Rapamycin

Fig. 10 Phosphatase SitA and Ppg1 are involved in regulating lipid droplet biogenesis.

(A) The intracellular lipid droplets were stained by boron dipyrromethene difluoride (BODIPY) in hyphae of the WT strain and observed under fluorescence microscopy. The phenotype of lipid droplets accumulation in the mycelia of the WT strain treated with or without 100 ng/mL rapamycin for 6 h (Bar, 10 μm).

(B) Phenotype of lipid droplets accumulation in the mycelia of the Δ*sch9* strain treated with or without 100 ng/mL rapamycin for 6 h (Bar, 10 μm).

(C) Phenotype of lipid droplets accumulation in the mycelia of the Δ*sitA* strain treated with or without 100 ng/mL rapamycin for 6 h (Bar, 10 μm).

(D) Phenotype of lipid droplets accumulation in the mycelia of the Δ*ppg1* strain treated with or without 100 ng/mL rapamycin for 6 h (Bar, 10 μm).

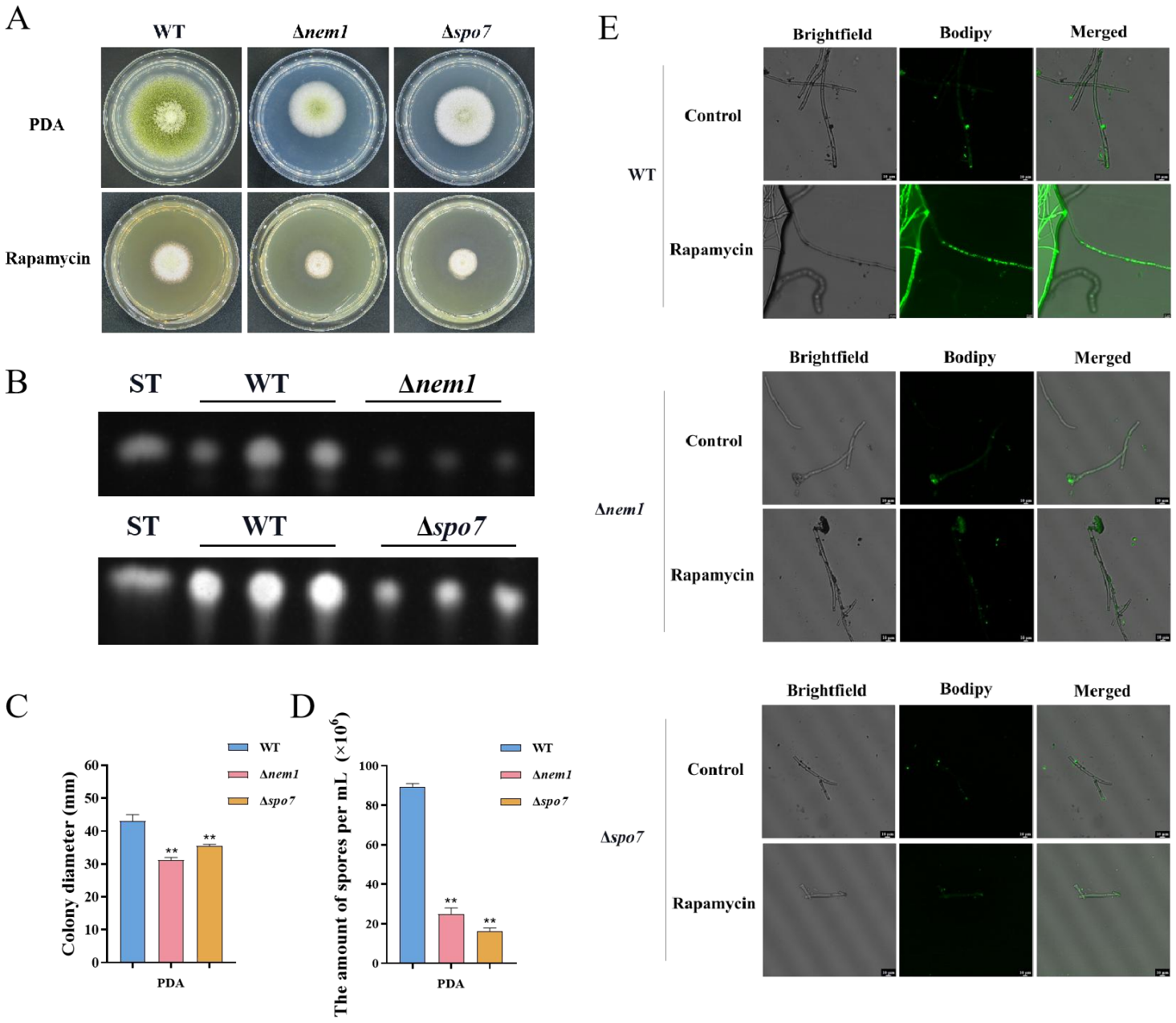
A
WT
Δnem1
Δspo7
PDA
Rapamycin
B
ST
WT
Δnem1
ST
WT
Δspo7
C
Colony diameter (mm)
WT
Δnem1
Δspo7
PDA
D
The amount of spores per mL (×10^6)
WT
Δnem1
Δspo7
PDA
E
Brightfield
Bodipy
Merged
WT
Control
Rapamycin
Δnem1
Control
Rapamycin
Δspo7
Control
Rapamycin

Fig. 11 Phosphatase complex Nem1/Spo7 play significant role in growth, conidiation, aflatoxin, and lipid droplet biogenesis.

(A) Phenotype of the WT, Δ*nem1*, and Δ*spo7* strains grown on PDA amended with 100 ng/mL rapamycin at 37°C for 5 days.

(B) TLC assay of AFB_1 production from the WT, Δ*nem1*, and Δ*spo7* strains cultured in YES liquid medium at 29°C for 6 days.

(C) Growth diameter of the WT, Δ*nem1*, and Δ*spo7* strains on PDA media.

(D) Statistical analysis of the sporulation by the WT, Δ*nem1*, and Δ*spo7* strains.

(E) Phenotype of lipid droplets accumulation in the mycelia of the WT, Δ*nem1*, and Δ*spo7* strains treated with or without 100 ng/mL rapamycin for 6 h (Bar, 10 μm).

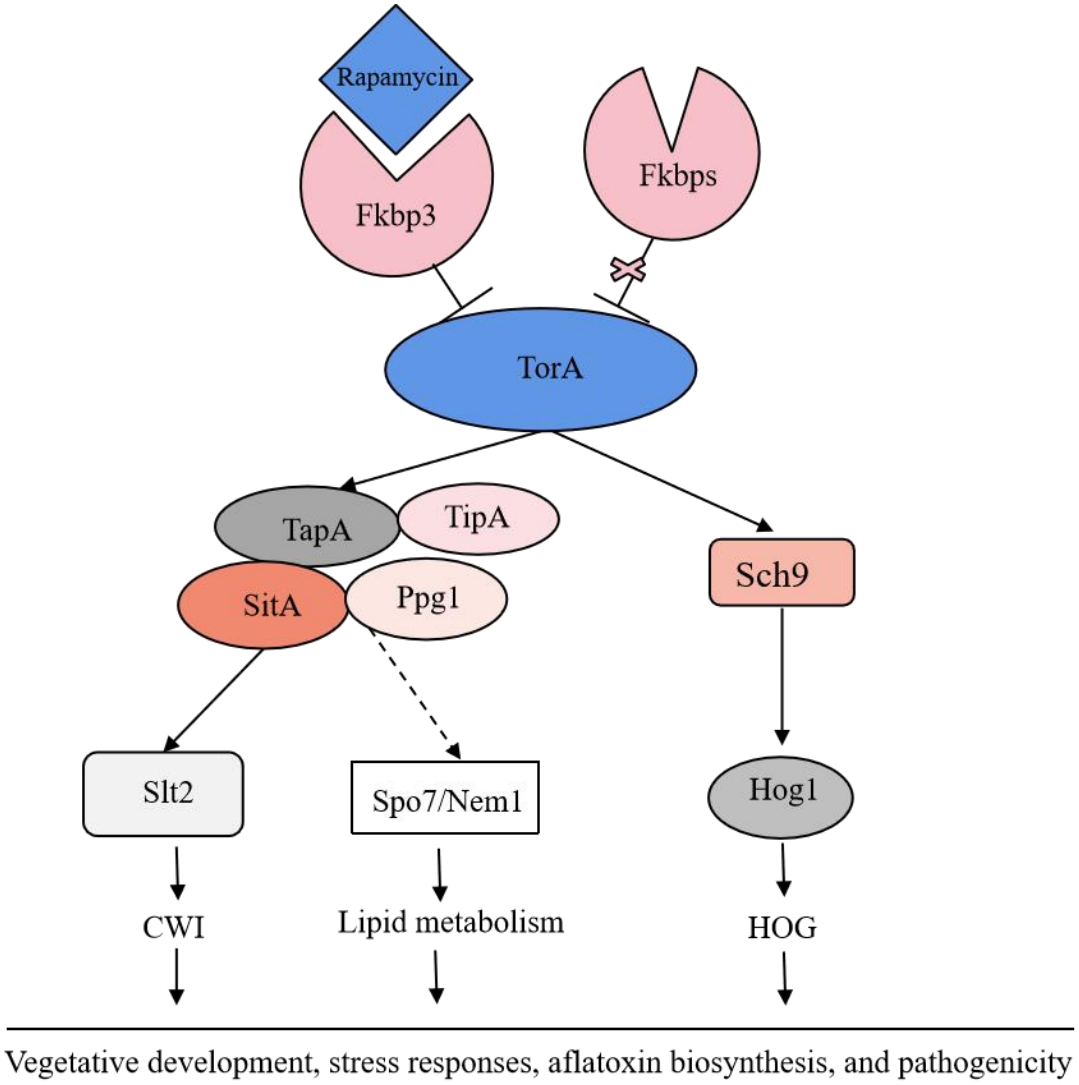
Rapamycin
Fkbp3
Fkbps
TorA
TapA
TipA
SitA
Ppg1
Sch9
Slt2
Spo7/Nem1
Hog1
CWI
Lipid metabolism
HOG
Vegetative development, stress responses, aflatoxin biosynthesis, and pathogenicity

Fig. 12 The proposed model of the target of rapamycin (TOR) pathway in *A. flavus*.

Based on the above results, we propose a hypothesis regarding the TOR signaling pathway model in *A. flavus.* Rapamycin forms a complex with Fkbp3, and this particular complex can bind to the TorA kinase, thereby impeding its regular functionality. Sch9, functioning as a downstream element of the TorA kinase, regulates aflatoxin biosynthesis and HOG signaling pathway. As another important target of the TorA kinase, TapA-phosphatase complex is involved in the regulation of growth, sporulation, sclerotia, aflatoxin production, CWI signaling pathway, lipid droplet synthesis, and other processes. In conclusion, the TOR signaling pathway plays a crucial role in various aspects of *A. flavus*, including vegetative development, stress response, aflatoxin biosynthesis, and pathogenicity.